SCHOOL OF ADVANCED STUDIES OF THE ROMANIAN ACADEMY

DOCTORAL SCHOOL OF CHEMICAL SCIENCES

"PETRU PONI"

INSTITUTE OF MACROMOLECULAR CHEMISTRY

CHEMISTRY Field

MASS SPECTROMETRY ANALYSIS OF CYCLIC MONOMER POLYMERIZATION

PhD THESIS SUMMARY

PhD supervisor:

Dr. Ing. Valeria HARABAGIU

PhD student:

BLAJ Diana-Andreea

2024

CONTENTS

INTRODUCTION

One of the most important challenges facing society today is the conservation of the planet. In the past decade, the focus on replacing finite fossil resources with biomass has intensified [1]. Biomass serves as a sustainable and renewable raw material for producing new materials with improved properties. Cyclodextrins (CDs), cyclic oligosaccharides derived from the enzymatic degradation of starch, are among the biomass-derived compounds. [2]. The most important property of CD is the ability to encapsulate hydrophobic molecules in the cavity through physical interactions, which leads to increased solubility of the guest molecule. This particularity recommends CD for a wide range of applications in water purification [3], catalysis [4,5], analytical chemistry [6], food industry [7], but especially in the pharmaceutical field [8-11] for increasing the water solubility of drug molecules.

On the other hand, native CDs have limited solubility, which is a disadvantage. Thus, chemical modifications of CDs become necessary to overcome this limitation. Among modified CDs, esterified derivatives are of particular importance due to their properties of biocompatibility, biodegradability, and low toxicity [12].

CD esterification (classical esterification, enzymatic esterification, or ring-opening polymerization reactions of lactones and lactides) leads to derivatives with various substitution degrees (SD) and positional isomers. This is a consequence of the high number of hydroxyl groups that can undergo substitution reactions (18, 21, or 24 in the case of α-, β-, or γ-CD) and their relatively similar reactivity (one-third being primary and two-thirds being secondary hydroxyl groups), making the structural analysis of these derivatives more difficult. CD modification by classical or enzymatic esterification (carboxylic acids, acid chlorides, anhydrides, or vinyl esters) typically results in the substitution of each hydroxyl group with one low-molecular-mass molecule. In contrast, oligomerization reactions of cyclic esters result in the formation of derivatives having multiple monomer units per active situs. Thus, the structural complexity of the sample may increase due to the molecular mass dispersity characteristic of oligomer substituents. These elements make the structural characterization of CD derivatives challenging, necessitating complex structural analysis methods to gain insight into the derivatization processes and the chemical structure of the compounds.

The development of mass spectrometry techniques with low ionization energy, particularly electrospray ionization (ESI) and matrix-assisted laser desorption/ionization

(MALDI) [13,14], has allowed a more precise structural characterization at the molecular level of compounds with complex architectures, such as CD derivatives. Over the last three decades, native CDs and their derivatives have benefited from mass spectrometry analysis which has been used to determine their molecular masses and distribution, identify the structure of attached units and terminal groups, and detect compounds resulting from side reactions [15-25].

In particular, MALDI MS is an important analytical method for determining the substitution degree of CD derivatives because it yields single-charged species as opposed to ESI which yields multiply-charged species. However, MALDI MS can provide biased information because of the mass discrimination effect in polymer samples with high molecular mass distributions [26]. Thus, it is necessary to validate the results using other analytical techniques. Nuclear magnetic resonance (NMR) spectroscopy is the most widely used technique for the structural analysis of CD derivatives to validate mass spectrometry data. However, NMR characterization of partially esterified CD derivatives can sometimes be difficult due to peak broadening and lack of standards for substituted CDs, requiring the use of complementary characterization techniques.

The utility of esterified CDs is enhanced by their modified solubility properties while retaining their ability to encapsulate hydrophobic molecules, which allows the preparation of inclusion complexes with a wide range of active principles. Therefore, various drugs (albendazole, acyclovir, lutein, cefradin, pindolol, and amoxicillin) have been encapsulated in esterified CDs [27-32]. On the other hand, CD modification with fatty acids leads to amphiphilic molecules that can form organized structures by self-assembly, resulting in biocompatible nano-aggregates, such as micelles [28,33,34], spheres [28,35], vesicles [29,36], and irregularly shaped rod-like or spherical particles with matricial or lamellar structures [37]. Additionally, amphiphilic CD derivatives can improve the transport of encapsulated drugs [38].

Esterified CDs can also be used as building blocks for biodegradable polymer networks [39-41], or can be electrospun without polymers to form fibers due to their high solubility [42]. Moreover, these types of derivatives have been used to transport heavy metals through membranes [43] or remove endocrine-disrupting chemicals from water [44]. Coatings for commercial polymers (polypropylene, polyethylene, polyethylene, polyvinyl chloride, polyurethane) have also been developed for industrial surface hydrophilization [45]. Due to the large number of sites that can be chemically modified, esterified CDs have also found

applications in macromolecular chemistry as initiators for ring-opening polymerization (ROP) [46-48] or radical atom transfer polymerization [49]. In addition, they can be used as photoinitiators or crosslinking agents when bis(acyl)phosphane oxide is attached to an esterified CD derivative [50].

Another research direction explores the CD's ability to form inclusion complexes with different guest molecules and can be exploited for regioselectivity control of substitution reactions [51]. For example, the transesterification reaction of vinyl and nitrophenyl esters, in the presence of CDs, leads to CDs esterified exclusively at the secondary hydroxyl groups [52]. The substitution selectivity is determined by the inclusion of the reactive species in the CD cavity at an early stage of the reaction. This interesting feature has been explored by performing the ring-opening reaction of cyclic esters in the presence of CD, leading to oligoester-modified cyclodextrins (CDOE). The CD influence in these reactions was demonstrated in the studies of Takashima *et al*, showing that cyclic esters undergo transesterification reactions with the secondary hydroxyl groups of CDs [46]. The exact mechanism has not yet been established, but the involvement of cyclic ester inclusion in the CD cavity has been shown [47].

In this context, the hypothesis guiding this PhD work consists of investigating ring-opening oligomerization (ROO) reactions in the presence of CD to gain a deeper understanding of CD's role in these reactions. Given the complexity of the structural characterization of CD-based compounds in different reaction phases, analytical methods will be optimized to accurately reflect the structural changes induced by various reaction parameters. Mass spectrometry plays an essential role in this work, generating precise information in the structural characterization of compounds resulting from ROO processes. At the same time, the PhD thesis aims to demonstrate the potential applicability of the synthesized compounds by developing new formulations for biomedical applications using the polymer-free electrospinning technique. Thus, an interdisciplinary approach integrating macromolecular chemistry, materials science, and medical bioengineering is emphasized.

The specific objectives underlying the PhD thesis are:

O1 – To monitor the influence of reaction parameters in the ring-opening process of cyclic esters (lactide - LA, lactones (ε-caprolactone - ε-CL, δ-valerolactone - δ-VL) initiated/catalyzed by β-CD on the structure and properties of CDOE derivatives by mass spectrometry, MS/MS and NMR spectroscopy;

O2 – To determine the behavior of two other homologs, α-, and γ-CD in ring-opening reactions of cyclic esters;

O3 – To assess the application potential of the synthesized CDOE derivatives by investigating the electrospinning process and their capacity to incorporate active principles.

The PhD thesis is composed of two main sections. **Part I** (**Chapter 1**) presents the scientific literature relevant to the thesis topic. **Part II** includes the original research and results obtained, and is structured in **Chapters 2-8**.

Chapter 1 provides an overview of general aspects related to the ring-opening oligomerization (ROO) process of cyclic esters and the kinetic investigation of this reaction. It also covers the modification of CDs with ester groups, the practical utility of the resulting derivatives, and the mass spectrometry characterization of polymers. Notably, it emphasizes the state-of-the-art research on the mass spectrometry characterization of esterified CDs.

Chapter 2 aims to extend the applicability of MALDI MS analysis by monitoring the reaction kinetics involved in the synthesis of β-cyclodextrin-oligolactide (β-CDLA) derivatives. Specifically, the MALDI MS technique was used to estimate the variations of the average molecular mass (*Mn*) over time for a better understanding of the chemical process. MALDI MS data were validated by measuring the monomer conversion using ^{1}H NMR spectroscopy. Additionally, the effect of reaction parameters was studied, specifically the influence of solvents such as dimethylformamide (DMF), dimethyl sulfoxide (DMSO), and N-methyl-2-pyrrolidone (NMP). By analyzing mass spectra and confirming structures through MS/MS fragmentation experiments, several secondary processes influencing the studied reactions were identified.

Chapter 3 proposes a new method for the MALDI MS quantification of transesterification processes in the ROO reaction of lactide. This method follows the evolution of the transesterification degree (*Tr*) in parallel with the mass of β-CDLA derivatives. Using β-CDLA synthesis as a model reaction system, the influence of various reaction parameters, particularly organocatalysts, on transesterification processes could be established. The developed MALDI MS method enables the comparative evaluation of lactide reaction systems by determining the relative transesterification rate (k_{Tr}^{app}). This approach proves to be useful for optimizing LA ring-opening processes, offering valuable data regarding the influence of reaction parameters on transesterification side reactions.

Chapter 4 presents the MALDI MS monitoring of the ROO reactions of ε-CL leading to the formation of β-cyclodextrin-oligocaprolactone (β-CDCL) derivatives. Initially, MALDI MS and ^{1}H NMR were employed to establish the conditions for MS analysis and validate the results. MALDI MS was further used to assess the influence of solvents and the effect of organocatalysts on the ROO of ε-CL. Additionally, the specific fragmentation profile resulting from gas-phase controlled collisional processes (MS/MS) was used to confirm the structure of different products detected by MALDI MS. The NMR study further correlated the increase in SD with the esterification site, demonstrating, for the first time in line with literature studies, the transfer of oligoesters from the larger to the smaller rim of β-CD molecules during ROO processes.

Chapter 5 explores the synthesis of β-CDCL derivatives in the presence of strongly nucleophilic bases at room temperature. The reaction kinetics are established by both MALDI MS and ^{1}H NMR spectroscopy. The study identifies the structural particularities of the resulting compounds and examines how different modes of substitution occur after specific reaction times with different organocatalysts. The optimized synthetic method allowed the preparation of β-CDCL derivatives selectively substituted at the large or small rim of the β-CD molecule. The experimental data led to a better understanding of the CD influence on the ring-opening process of ε-CL.

Chapter 6 presents the ROO process of δ-VL in solution using β-CD and strongly nucleophilic organocatalysts. The reactions were monitored by MALDI MS and ^{1}H NMR spectroscopy, showing a good agreement between the two methods. Transesterification reactions were also observed in these organocatalyzed systems by both analytical methods. In this case, NMR characterization revealed the exclusive substitution at the smaller rim of β-CD, contrary to the mode of substitution reported in the literature for the bulk processes. Kinetic studies enabled the differentiation of reactivity associated with monomer activation through inclusion in the CD cavity.

Chapter 7 explores the applicability of CDOE derivatives by investigating the electrospinning process and the incorporation capacity for different biologically active compounds. The main aspects consist of determining the optimal conditions for producing nanofibers from CDOE derivatives and incorporating active principles using the electrospinning process, without the use of additional polymers to facilitate the process. Thus, the study highlights, for the first time, the possibility of obtaining pharmaceutical formulations of active

principles in the form of nanofibers (curcumin – CRC, magnolol – MG, honokiol – HK, enrofloxacin – ENR) using CDOE compounds. The morphology of different systems is examined by scanning electron microscopy (SEM) to confirm the fiber formation, while dynamic water vapor sorption (DVS) studies assess the hygroscopicity. Analytical methods such as NMR and Fourier transform infrared spectroscopy (FTIR) are employed to confirm the presence of bioactive compounds in the corresponding fibers. Additionally, the antioxidant and antibacterial properties of the formulations are validated through further testing.

Chapter 8 presents the materials, synthesis, and characterization procedures used throughout the thesis. The electrospinning technique and nanofiber characterization methods are also described.

The PhD thesis concludes with a summary of the general conclusions drawn from the conducted studies, highlights the key aspects of the scientific work disseminated during the doctoral research, and includes the bibliography referenced throughout the thesis.

PERSONAL CONTRIBUTIONS

2. MONITORING THE SYNTHESIS OF CYCLODEXTRIN-OLIGOLACTIDE DERIVATIVES BY MALDI MASS SPECTROMETRY

The ROO of LA in the presence of β-CD (**Scheme 2.1**) leads to the modification of oligosaccharide with oligoester chains especially at the small rim of β-CD, which contains primary hydroxyl groups [32,160]. The mass spectra contain various series of signals having a peak-to-peak increment of 144 or 72, specific for OLA chains (**Figure 2.4**). The presence of multiple signal series is a result of the formation of β-CDLA with different structures. **Table 2.2** shows the equations corresponding to peak series having specific β-CDLA structures.

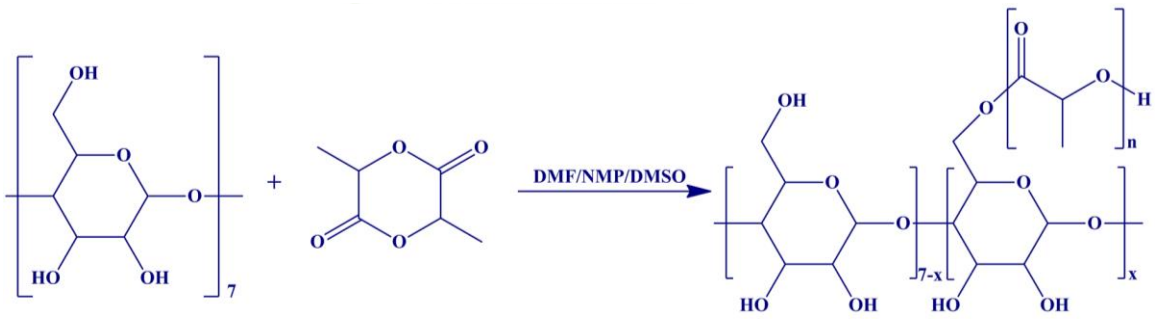

Scheme 2.1. *Ring-opening oligomerization of LA in the presence of β-CD*

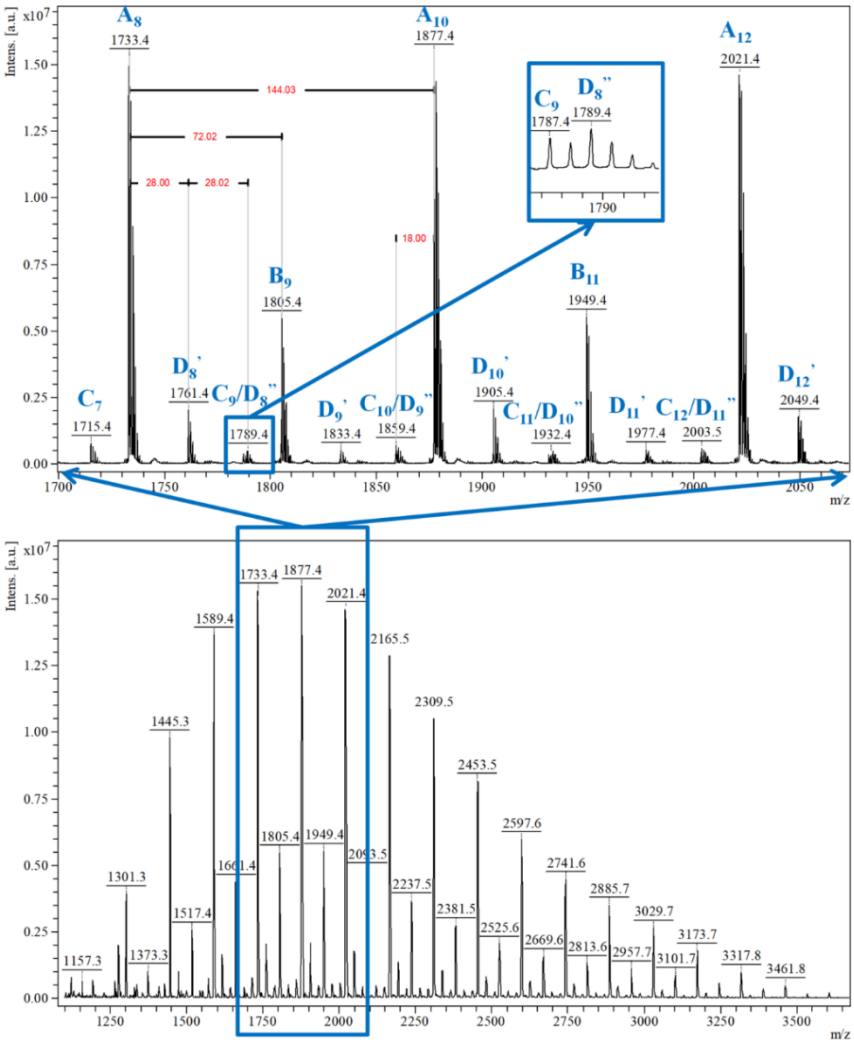

Figure 2.4 *MALDI MS mass spectra for β-CDLA#11 – peak annotation was performed according to the equations in* ***Table 2.2***

Table 2.2 *Equations used to assign the corresponding monoisotopic β-CDLA peaks from MALDI MS spectra*

Series	***m/z***
A[a]	*72 x n (lactate) + 1134 (β-CD) + 23 (Na^+)*
B[b]	*72 x n (lactate) + 1134 (β-CD) + 23 (Na^+)*
C	*72 x n (lactate) + 1134 (β-CD) + 23 (Na^+) + 54 (acrylate)*
D	*72 x n (lactate) + 1134 (β-CD) + 23 (Na^+) + 28 (formate)*
E[c]	*72 x n (lactate) + 1134 (β-CD) + 23 (Na^+) + 97 (4-(methylenimino)butanoate)*
F[c]	*72 x n (lactate) + 1134 (β-CD) + 23 (Na^+) + 100 (4-(methylenamino)butanoate)*

[a]even number of dairy units
[b]odd number of dairy units
[c]observed in the mass spectra of β-CDLA synthesized in NMP (#13)

2.2.1. Optimization and validation of MALDI MS analysis conditions

To observe the matrix effects on *Mn* evolution, MALDI MS spectra of β-CDLA samples collected from the reaction mixture were registered using CHCA (thin layer) or DHB (dry droplet). Quantitatively, there are no significant differences in the *Mn* evolution determined by MALDI MS with the two matrices (**Figure 2.6a**). However, for reaction times longer than 48 h (i.e., for samples with more than 5 LA units attached), the *Mn* values calculated from CHCA analysis are slightly higher. This discrepancy in *Mn* values between samples prepared with DHB and CHCA may result from differences in the β-CDLA solubility in the respective solvents as the mass increases.

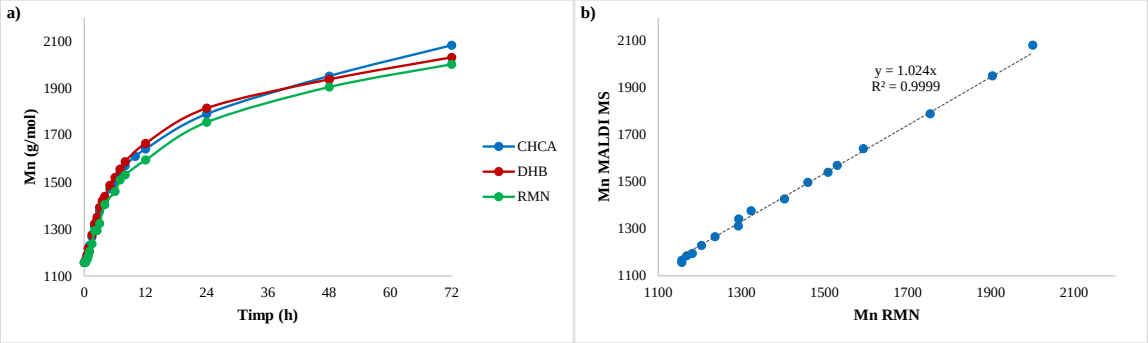

Figure 2.6. *a) Mn evolution of β-CDLA$_{\#3}$ by MALDI MS (CHCA and DHB) and ^{1}H NMR; b) agreement between Mn evolution determined by MALDI MS (with CHCA matrix) and ^{1}H NMR*

Considering that sample preparation with CHCA matrix is more suitable for β-CDLA analysis, it was used to determine the kinetics of ROO reactions by MALDI MS. The results on the evolution of *Mn* values obtained by analyzing the MALDI MS spectra were validated using the monomer conversion by ^{1}H NMR. The comparative graphical representation of *Mn* values resulting from the two methods reveals the accuracy of the determination performed by the MALDI MS technique, with y = 1.024 x and R^2 = 0.99 (**Figure 2.6b**). Previous studies on PLA, comparing *Mn* values obtained by MALDI MS with those measured by SEC, primarily focused on the evolution trend of *Mn* values over time [100]. Although a linear dependence was determined between the values obtained by SEC and MALDI MS, due to the relative values obtained by SEC, the Mn_{SEC} values were 1.5 times higher compared to $Mn_{MALDI\ MS}$.

2.2.4. Influence of reaction temperature

The reaction time can be shortened either by increasing the reaction temperature or by adding ROP organocatalysts [72,74,112,283]. Thus, the effect of temperature on the ROO process was investigated by MALDI MS, showing the *Mn* evolution for reaction systems conducted at different temperatures (80, 100, 120 °C) (**Figure 2.12a**).

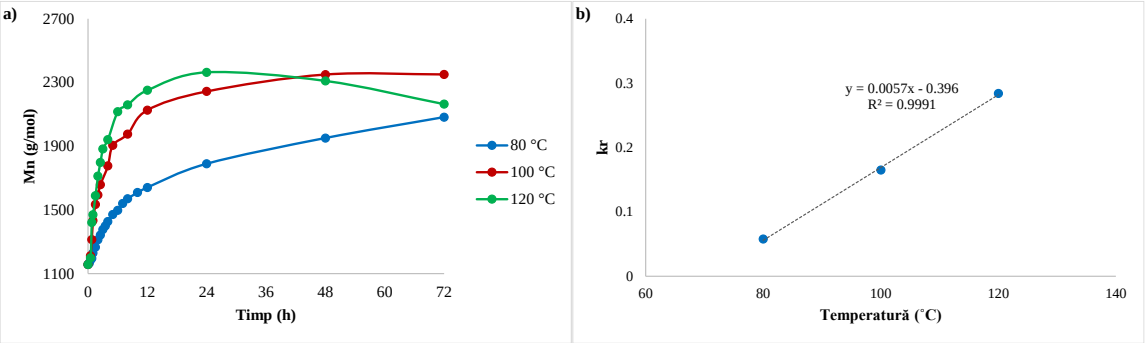

Figure 2.12. *a) Influence of temperature on the Mn values of β-CDLA in DMF; b) variation of the apparent reaction rate (k_r) with temperature (#3,8,11)*

The two-step increase of *Mn* is observed for all temperatures but in a different way. The Mn evolution shows an initial increase that is accelerated at higher temperatures, followed by a slower increase or even a decrease at 120 ˚C. Analysis of the MALDI MS spectra indicates that higher temperatures allow the maximum *Mn* values to be reached more quickly, within 48 h at 100 ˚C and 24 h at 120 ˚C (**Figure 2.12a**). The apparent reaction rate (k_r) values increase significantly from 80 °C (k_r = 0.058) to 100 °C (k_r = 0.165) and 120 °C (k_r = 0.284). The k_r values, calculated over the linear increase of *Mn* (0 to 8 h), were plotted against the reaction temperature (**Figure 2.12b**). The k_r increases linearly with temperature, confirming that the ring-opening process is primarily driven by a single type of initiator. However, the reaction system deviates from first-order kinetics after 8 h, likely due to steric hindrances caused by the increase in SD and the occupation of active sites.

The *Mn* evolution at 120 °C (**Figure 2.12a**) shows that β-CDLA undergoes depolymerization reactions after reaching the maximum value at 24 h. The *Mn* reduction indicates an intensification of transesterification reactions or other thermally activated degradation processes involving the OLA chains in the product. In addition to transesterification reactions, other processes that are influenced by the reaction temperature were observed in the mass spectra of the β-CDLA$_{\#11}$ product obtained at 120 °C (*C* and *D* series– **Figure 2.4**). The

structure of the side products was confirmed by MS/MS fragmentation, as these products were present in too low amounts to be detected by NMR. The *C series* can be associated with the degradation of the OLA chains by water elimination [107,287], resulting in a β-CDLA product with acrylate end groups (**Scheme 2.2**).

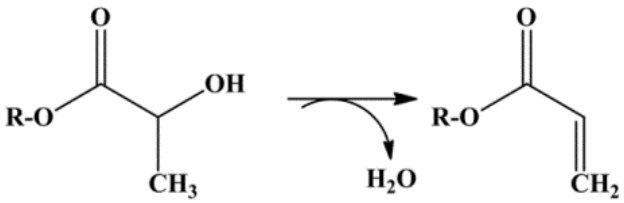

Scheme 2.2. *Water elimination from OLA chains*

2.2.5 The role of DMF as a solvent for ROO

The selection of solvents for a ROO reaction involving both β-CD and LA is quite limited, so DMF, NMP, and DMSO were considered. In this context, it is important to determine the role of DMF in the synthesis of β-CDLA, specifically whether DMF acts as an activator in the conversion of LA. The *Mn* evolution evaluated at 80 ˚C indicates that using solvents other than DMF affects the maximum values (**Figure 2.16**). Regardless of the solvent, the *Mn* evolution has two increase stages: an initial stage of rapid growth up to about 20 h, followed by a second stage of slow growth. At the same time, for later stages of the reaction (over 20 h), the *Mn* values remain relatively constant in DMSO and NMP, while a slow but continuous increase is observed in DMF. This behavior can be attributed to the activation of newly formed secondary hydroxyl groups only in the case of DMF, similar to the activation mechanism of ROP reactions in the presence of organocatalysts.

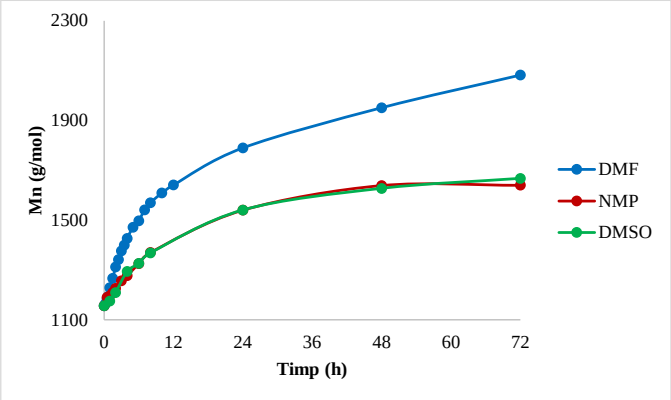

Figure 2.16. *Solvent influence on Mn values of β-CDLA at 80 °C (#3, 12, 15)*

The cleavage of the amide bond of DMF with dimethylamine formation can occur in the presence of hydroxyl groups (**Scheme 2.5**) [291]. The dimethylamine can influence the ROO process, similarly to organocatalysts [72], by activating the nucleophilic attacks of hydroxyl groups; this activation explains the higher value of k_r observed for reactions conducted in DMF. The formation of dimethylamine is also supported by the pale-yellow color of the reaction mixture after 72 h. The cleavage of the DMF amide bond may account for the appearance of *D series* (CDLA-formate species) in the mass spectra of β-CDLA products, confirmed by MS/MS analysis.

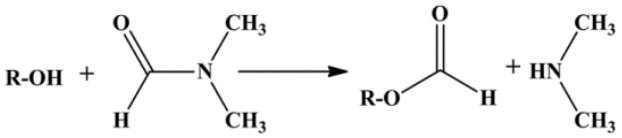

Scheme 2.5. *DMF amide bond cleavage*

3. QUANTIFICATION OF TRANSESTERIFICATION REACTIONS IN CYCLODEXTRIN-OLIGOLACTIDE SYSTEMS BY MALDI MS

3.2. Investigation of transesterification reactions in the synthesis of β-cyclodextrin-oligolactide derivatives

The ROP process of LA in the presence of β-CD as an initiator, with or without the addition of organic catalysts, was considered a case study for the development of a new method for the quantification of transesterification reactions by MALDI MS mass spectrometry. **Scheme 3.1** shows transesterification reactions that can occur in these types of systems.

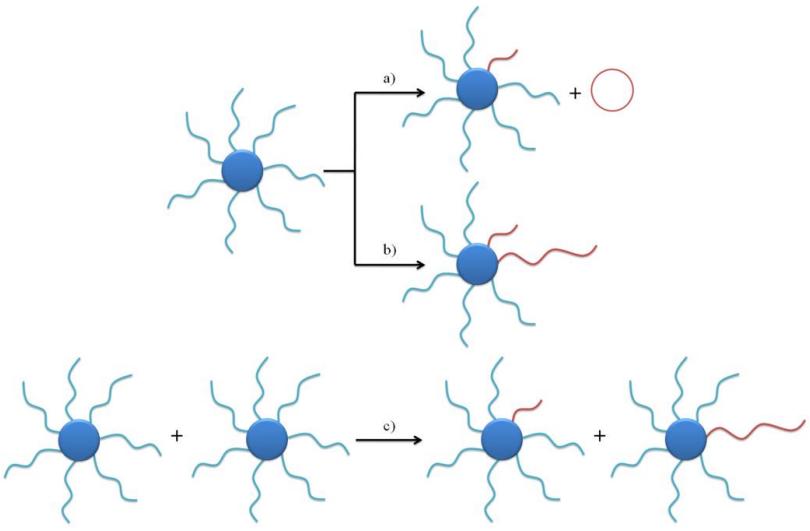

Scheme 3.1. *Transesterification reactions in β-CDLA systems: a) backbiting reaction, b) intramolecular exchanges, and c) intermolecular exchanges*

The method for quantifying transesterification reactions relies on analyzing the mass spectra of β-CDLA samples collected at specific reaction times. This approach allows the quantification of the transesterification degree (*Tr*) by examining two series of peaks: a main, higher intensity series with peak-to-peak differences of 144 Da corresponding to products formed as a result of the ROP process (*A series* in **Figure 2.4**), and a series of lower intensity peaks with differences of 72 Da, associated with transesterification reactions (*B series* in **Figure 2.4**). In **Figure 3.1**, the signals highlighted in blue are associated with β-CDLA species having an even number of lactate units (*A series*), and the signals highlighted in red correspond to species with an odd number of lactate units (*B series*).

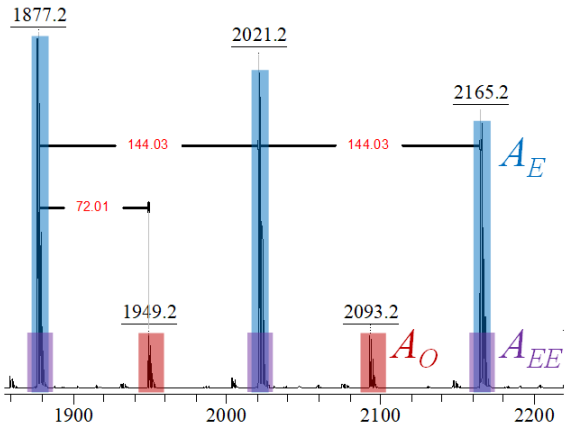

Figure 3.1. *Enlarged area of the mass spectrum corresponding to a β-CDLA derivative*

It can be assumed that the transesterification processes leading to β-CDLA species with an odd number of monomer units simultaneously generate an equivalent number of β-CDLA species with an even number of monomer units (as depicted in **Figure 3.1** in purple). Therefore, both peaks corresponding to the odd number of monomer units and the equivalent part of peaks with an even number were considered for more accurate quantification of *Tr*. Thus, the relative *Tr* can be calculated using the following equation:

$$Tr = \frac{\sum A_{TR}}{\sum A_{total}} * 100 = \frac{\sum(A_O + A_{EE})}{\sum(A_O + A_E)} * 100 \qquad (3.1)$$

The *Tr* evolution for the β-CDLA synthesis reaction in the presence of DMAP shows an increase of *Tr* values up to 30% (**Figure 3.3a**). These values result from two simultaneous chemical processes evidenced by the MS characterization: the ring-opening of LA, which decreases the *Tr* (increase in MS peaks corresponding to species with an even number of lactate units), and transesterifications, which increase the *Tr* (increase in MS peaks corresponding to

species with an odd number of lactate units). The comparative plot of *Mn* and *Tr* values reveals that transesterification processes continue to occur even when *Mn* values remain constant, indicating that *Tr* is not affected by the ROO process. To correlate the prevalence of transesterification reactions with the reaction conditions, the relative transesterification rate (k_{Tr}^{app}), which can be defined as the time variation of the transesterified β-CDLA species (**Figure 3.3b**) and can be calculated using the following formula:

$$k_{Tr}^{app} = \frac{d(ln\frac{(x_{CDLA})_o}{(x_{CDLA})_0 - (x_{CDLA})_{Tr}})}{dt} \quad (3.2)$$

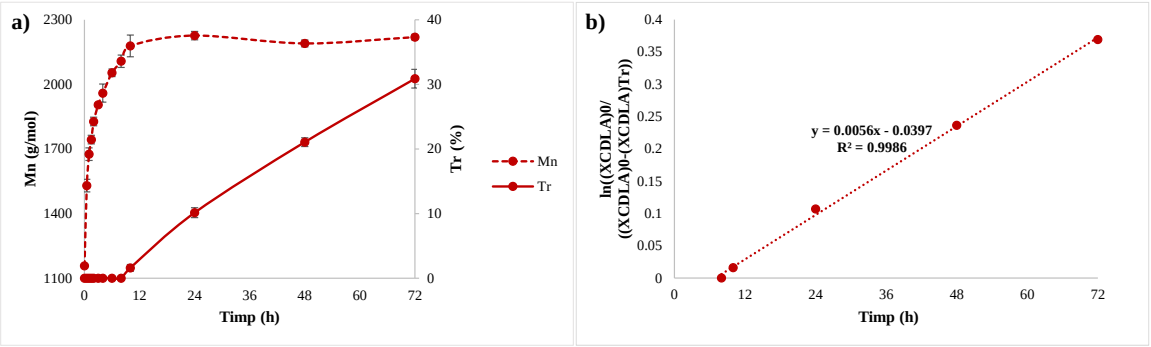

Figure 3.3. *a) Evolution of Mn and Tr values and b) the semilogarithmic plot used to calculate k_{Tr}^{app} for the β-CDLA synthesis reaction in the presence of DMAP (#19)*

The k_{Tr}^{app} value can be considered an apparent rate constant for the transesterification reactions, assuming that *Tr* accurately reflects the concentration of transesterified species in the reaction mixture. In an ideal reaction, the k_{Tr}^{app} value is 0, indicating the absence of transesterification reactions in the system. Any deviation from this ideal value signifies the occurrence of transesterification processes, whether they involve backbiting, intra-, or intermolecular exchange.

3.2.1. Influence of temperature and solvent

Previous studies have demonstrated that increasing the reaction temperature causes an increase in the incidence of transesterification reactions [62,63,68,112]. In DMF at 80 °C, the incidence of transesterifications is influenced by the reaction temperature in the order: $k_{Tr}^{app}{}_{80}$ (0,51) < $k_{Tr}^{app}{}_{100}$ (6,17) < $k_{Tr}^{app}{}_{120}$ (11.9) (**Figure 3.6**). Therefore, the prevalence of transesterification reactions increases with increasing temperature, in line with previous studies [68,115]. The optimization study of β-CDLA synthesis must focus on minimizing *Tr* while

achieving the highest possible *Mn*. As the β-CD molecules are modified, a decrease in the LA conversion rate is observed while maintaining a constant *Tr* evolution (linear *Tr*, especially for 80°C). This suggests that the variation in *Tr* is independent of the LA ROO process rate and is likely related to the incidence of transfer reactions between the different binding sites on the β-CD molecule. The increased length of OLA chains favors, in addition to the interchange transesterification reactions, the backbiting reaction, with *Mn* reduction as observed for the reaction at 120°C.

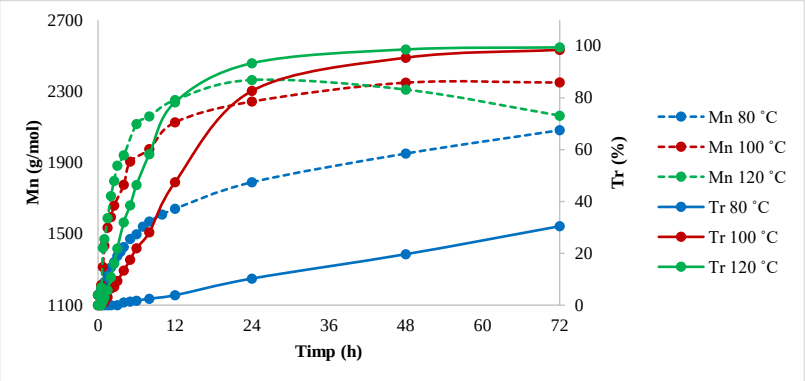

Figure 3.6. *Temperature influence on Mn and Tr evolution for DMF systems (#3, 8, 11, **Table 2.1**)*

3.2.3. Influence of total reactant concentration

The influence of the total reactant concentration (g/mL) in DMF at 80 °C (**Figure 3.12**) showed that differences are minimal, $k_{Tr}^{app}{}_{0.1}$ (0,46) < $k_{Tr}^{app}{}_{0.2}$ (0,48) < $k_{Tr}^{app}{}_{0.4}$ (0.51), which indicates that intramolecular transesterification reactions (on the same β-CD molecule) are the predominant process.

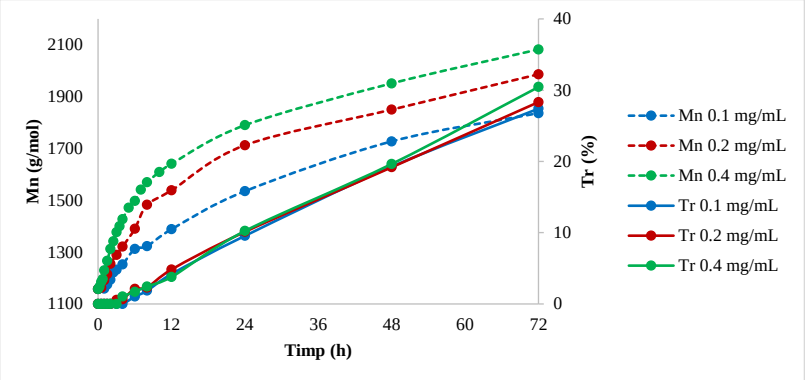

Figure 3.12. *Total reactant concentration influence on Mn and Tr evolution for reactions conducted in DMF at 80 °C (#1-3, **Table 2.1**)*

3.2.4. Influence of organocatalysts

The determination of k_{Tr}^{app} using the MALDI MS method established the following order of transesterification reactivity: $k_{Tr}^{app}{}_{imidazole}$ (0,09) < $k_{Tr}^{app}{}_{DMAP}$ (0,56) < $k_{Tr}^{app}{}_{(-)\text{-}sparteine}$ (12.1) (**Figure 3.14**). It was considered useful to compare the reaction systems at the point when the maximum *Mn* value is reached. In the case of imidazole, at a maximum *Mn* of 2180 g/mol, the *Tr* value is only 5%, whereas for DMAP at *Mn* of 2215 g/mol, the *Tr* value reaches 10%. However, the reaction time required for the imidazole system is significantly longer. When optimizing the process for maximum *Mn* with minimal *Tr*, it is observed that (-)-sparteine leads to higher *Tr* compared to DMAP. Thus, activation using DMAP turns out to be the ideal solution considering both *Tr* and *Mn* values. In contrast, when considering the duration of the reaction process, (-)-sparteine may represent the optimal solution. After 3 h reaction time, (-)-sparteine leads to *Mn* and *Tr* values of 2145 g/mol and 31.5%, respectively.

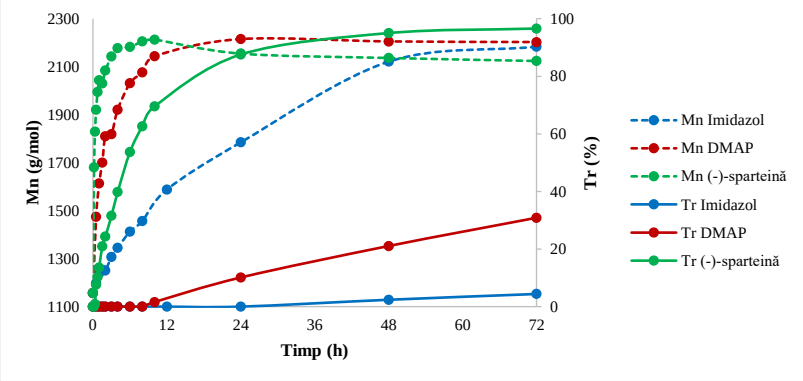

Figure 3.14. *Tr and Mn evolution using different organocatalysts (#18 - imidazole, #19 - DMAP, #22 - (-)-sparteine, **Table 2.1**)*

3.3. Investigation of transesterification processes involved in the organocatalytic degradation of β-CDLA

The same β-CDLA product was subjected to degradation in the presence of different organocatalysts to detect their involvement in *Mn* reduction processes through macrocycle formation. The product has a relatively high *Mn* value (3750 g/mol) and a low *Tr* value (11.65%). The trend observed for the three organocatalysts ($k_{Tr}^{app}{}_{imidazole}$ (2.02) < $k_{Tr}^{app}{}_{DMAP}$ (8,93) < $k_{Tr}^{app}{}_{(-)\text{-}sparteine}$ (92.65)), is consistent with the analysis of the ROO process, as shown in **Figure 3.18**. With (-)-sparteine, *Tr* reaches its maximum value in only 4 h, but transesterification reactions continue beyond this period, as indicated by the continuous decrease in *Mn* values. A significant decrease in *Mn* up to 3400 g/mol is also observed in the presence of DMAP, with *Tr*

reaching 51%, but over a longer period than (-)-sparteine. On the other hand, imidazole leads to the least pronounced degradation of the β-CDLA product, with the *Mn* value reaching 3700 g/mol. This organocatalyst results in a modest increase in *Tr*, reaching 23% in 8 h.

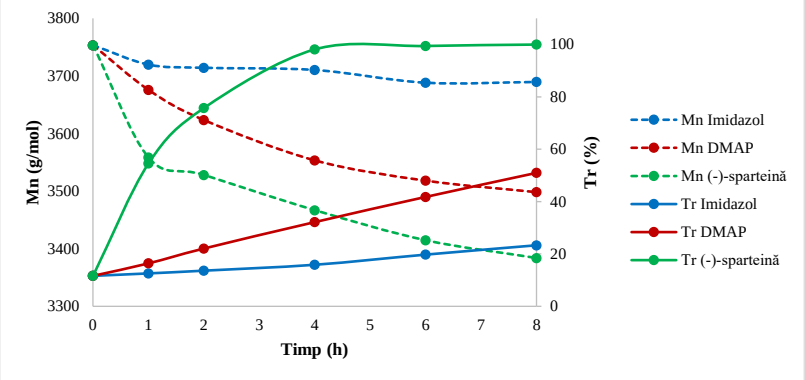

Figure 3.18. *Mn and Tr evolution in the β-CDLA product with different organocatalysts (imidazole, DMAP, (-)-sparteine) at 80 °C in DMSO*

4. SYNTHESIS AND ADVANCED STRUCTURAL CHARACTERIZATION BY MALDI MS OF CYCLODEXTRIN-OLIGOCAPROLACTONE DERIVATIVES

β-CDCL derivatives were synthesized through the ring-opening reaction of ε-CL in the presence of β-CD and two organocatalysts (DMAP and (-)-sparteine; **Scheme 4.1**). The mass spectrum of a typical β-CDCL product, obtained in the presence of DMAP, is shown in **Figure 4.1**. The mass spectrum consists of a series of peaks with 114 Da differences (corresponding to the CL monomer units) starting from the signal at *m/z* 1157, corresponding to the sodium adduct of β-CD. MS/MS fragmentation studies confirmed the structural characterization of β-CDCL products.

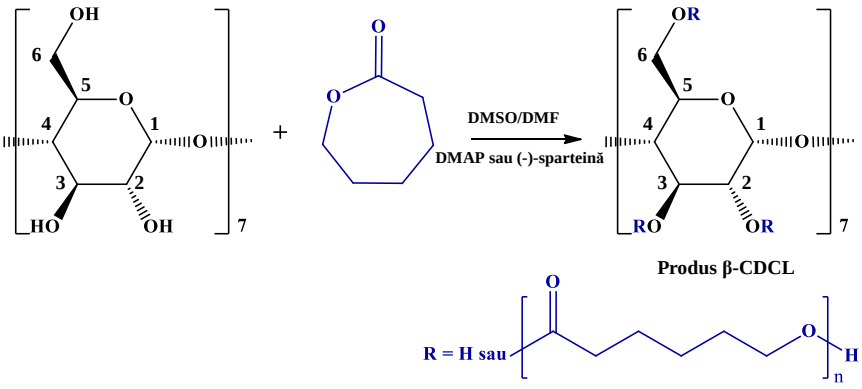

Scheme 4.1. *The ring-opening reaction of ε-CL initiated by β-CD*

The COSY experiment revealed signals for two glucopyranose units of β-CD, substituted differently at positions 3 and 2. This substitution pattern is important for understanding the mechanism of ε-CL ring-opening in the presence of β-CD. Specifically, for substitution at C2, the H2 signal appears at 4.42 ppm, with the corresponding H3 signal in the vicinity at 3.88 ppm (as shown in **Figure 4.7**). For substitution at C3, the H3 signal is observed at 5.13 ppm, with the corresponding H2 signal around 3.4 ppm.

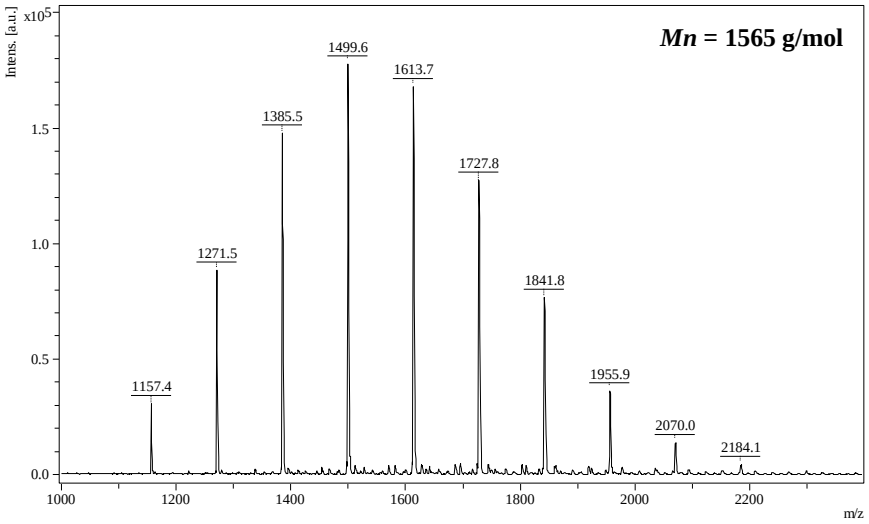

Figure 4.1. *MALDI MS mass spectrum of a typical β-CDCL product#2*

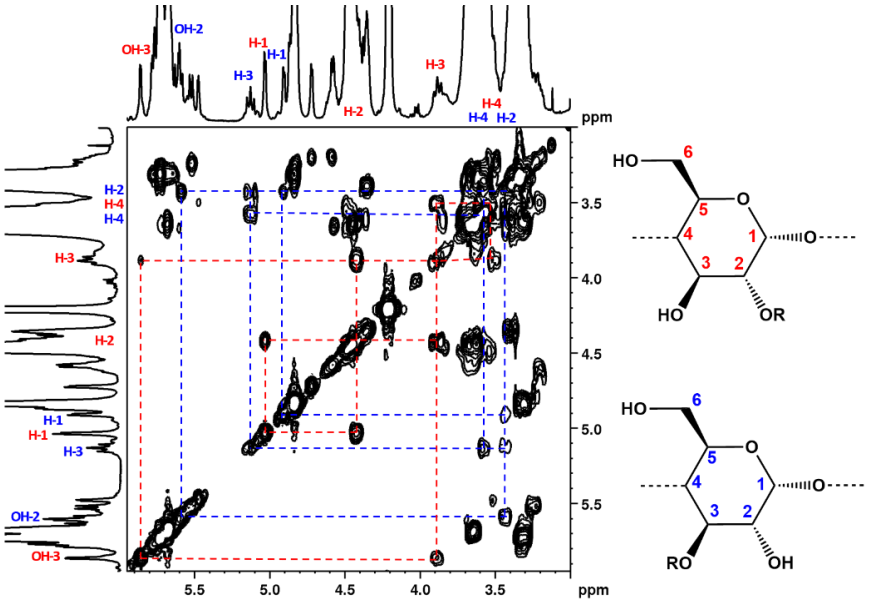

Figure 4.7. *COSY experiment (DMSO-d6, 400 MHz) showing substitutions at C2 (red) and C3 (blue)*

In the ^{1}H NMR spectra of the reaction sample collected after 6 h, a signal corresponding to the methylene group in the ε-position of the CL appears at 3.99 ppm. Although this peak partially overlaps with a satellite signal for CH2-ε of the unreacted ε-CL, its presence is confirmed by the COSY experiment due to its coupling with chain CH2-δ (**Figure 4.8a**). Additionally, for the sample collected after 11 h, the NMR spectrum shows signals corresponding to the two H6′ protons of the glucopyranose units of β-CD, substituted at the hydroxyl groups in position 6. These broad peaks partially overlap with others, but their presence is confirmed by correlations with C6′ at 63.2 ppm in the HSQC spectrum (**Figure 4.8b**). This indicates that the substitution also occurs at position 6 after a certain reaction time.

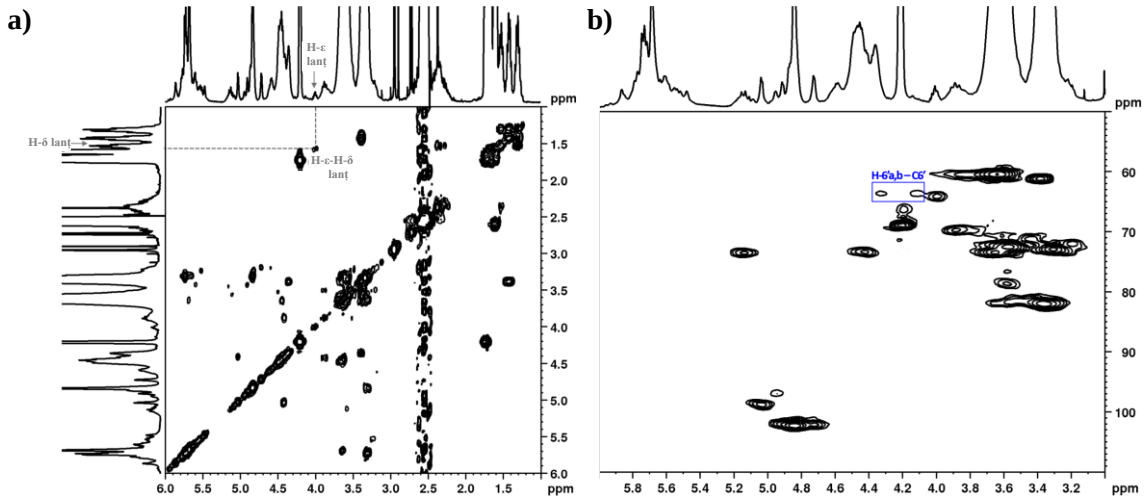

Figure 4.8. *a) COSY spectrum (DMSO-d6, 400 MHz) for the sample β-CDCL collected after 6 h and b) HSQC spectrum (DMSO-d6, 400 MHz) for the sample β-CDCL collected after 11 h*

4.2.3. Kinetics of the β-CDCL synthesis determined by MALDI MS and NMR

The kinetics of the ε-CL ring-opening reaction using β-CD as initiator and DMAP as organocatalyst (#2) was monitored by both MALDI MS using DHB or CHCA as a matrix for sample preparation and ^{1}H NMR spectroscopy to confirm the obtained results. The evolution of Mn_{RMN} and Mn_{MALDI} obtained using both DHB and CHCA matrices is shown in **Figure 4.10a**. An excellent agreement between NMR and MALDI MS using DHB as a matrix is observed, with a similar *Mn* evolution, reaching 1600 g/mol at the end of the reaction time, corresponding to 3.85 CL monomer units per β-CD molecule. Furthermore, the plot of *Mn* values determined by MALDI MS using DHB and ^{1}H NMR was characterized by a linear evolution with $y = x$ and $R^2 = 1$ (**Figure 4.10b**).

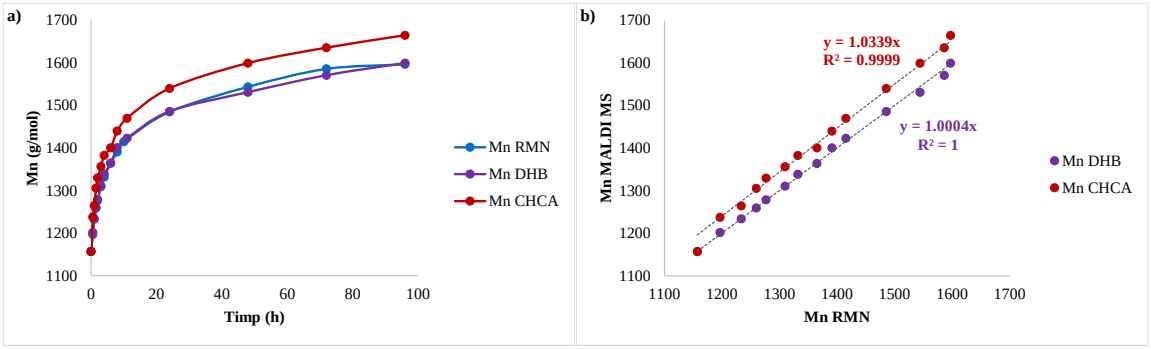

Figure 4.10. *a) Mn evolution for β-CDCL$_{\#2}$ determined by MALDI MS (using DHB or CHCA) and ^{1}H NMR; b) the correlation between the evolution of equivalent Mn values determined by ^{1}H NMR and MALDI MS (using DHB and CHCA)*

Another important element, in evaluating the β-CD modification reaction, is the monomer consumption rate profile. Thus, two obvious regions were observed (**Figure 4.10a**): the first, up to 12 h, was characterized by a rapid monomer conversion, with 2.3 CL units being attached to β-CD during this time. For the second region from 12 to 96 h, the conversion was much slower, with an increase in *Mn* of only 1.5 CL units. In addition, NMR analysis showed that the overall β-CD substitution pattern changed during the reaction; in the first step of fast monomer conversion, substitution occurred at positions 2 and 3, while in the second step, the esterification could also be observed at position 6.

4.2.5. Influence of organocatalysts in the β-CDCL synthesis determined by MALDI MS

The *Mn* evolution of DMAP and (-)-sparteine-catalyzed reactions were compared with those without catalysts. The kinetic study of the reaction conducted only in DMSO shows a low ε-CL conversion, with *Mn* reaching only 1400 g/mol (**Figure 4.16**). In the DMAP/DMSO system, after a rapid initial increase, *Mn* values increase slowly and continuously, reaching 1600 g/mol at the end of the reaction time. Even in the reaction system with (-)-sparteine, a stronger nucleophilic activator, the conversion was not complete. *Mn* values increased rapidly up to 12 h, and afterward, *Mn* remained constant or decreased due to backbiting reactions.

The kinetic analysis of DMF reactions revealed a similar behavior (**Figure 4.17a**), with the same order of reactivity (-)-sparteine > DMAP > no organocatalyst. Comparing the evolution of *Mn* values, it is evident that the reaction systems in DMF are significantly more active than those in DMSO. This increased activity is likely due to degradation processes in DMF that generate the nucleophilic activator dimethylamine.

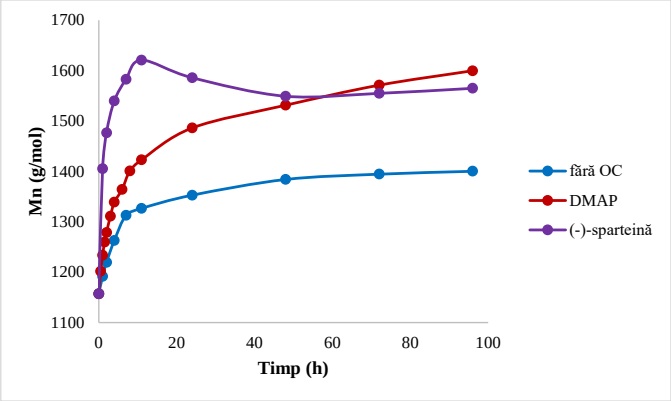

Figure 4.16. *Organocatalyst influence on Mn evolution in DMSO (#1-3)*

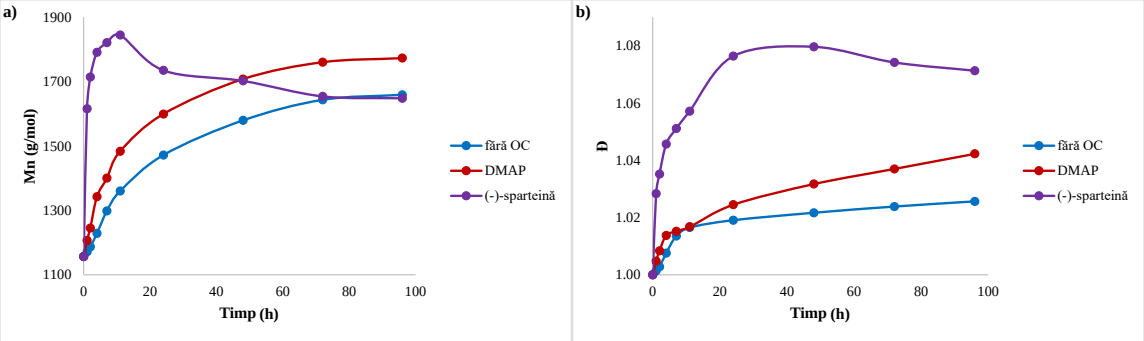

Figure 4.17. *a) Organocatalyst influence on Mn evolution in DMF and b) the evolution of the dispersity index (#4-6)*

The Đ evolution determined by MALDI MS can further reveal differences in reactivity within the system. The system with (-)-sparteine reached the same *Mn* value in 4 h as the system with DMAP at the end of the reaction. However, the dispersity obtained with DMAP was significantly lower (**Figure 4.17b**).

5. CONTROLLED MODIFICATION OF CYCLODEXTRIN BY RING-OPENING OLIGOMERIZATION OF ε-CAPROLACTONE IN THE PRESENCE OF TBD AND DBU ORGANOCATALYSTS

The selective substitution at the secondary hydroxyl groups of the β-CD molecule may be favored by inclusion phenomena and differences in the reactivity of hydroxyl groups in transesterifications. The encapsulation of ε-CL in the β-CD cavity in DMSO was demonstrated by the appearance of NOE correlation signals between ε-CL protons and H3/H5 protons of the β-CD cavity (**Figure 5.2**) when the monomer was added in an excess according to the reaction conditions. Based on previous studies on the geometry of β-CD:ε-CL complexes formed in

water [47, 306], one can assume the spatial proximity between the carbonyl function of ε-CL and the larger rim of β-CD in DMSO, as illustrated in **Figure 5.2**.

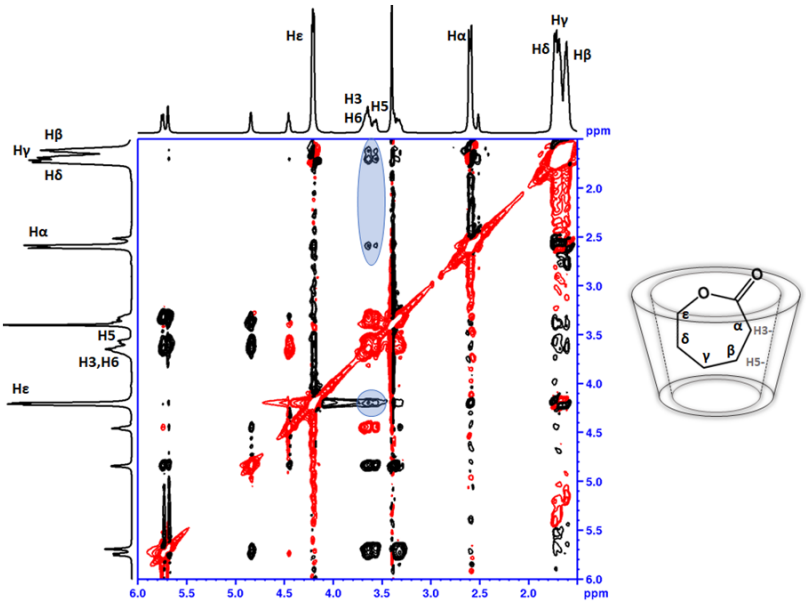

Figure 5.2. *ROESY spectrum (DMSO-d6, 400 MHz) for a β-CD/ε-CL 1/20 mixture highlighting the NOE correlation signals between H3/H5 of β-CD and ε-CL protons*

The ROO process of ε-CL initiated by β-CD was performed in DMSO at 80 °C for 72 h. The mass spectrum of the **β-CDCL$_{\#1}$** product allowed the *Mn* quantification (1425 g/mol), corresponding to the attachment of 2.35 CL units to β-CD. The ^{1}H NMR analysis confirmed the total number of CL units/β-CD. Additionally, the NMR analysis of the β-CDCL$_{\#1}$ indicated selective substitution at the larger rim.

5.2.3. Comparative ^{1}H NMR and MALDI MS studies for the ROO process of ε-CL organocatalyzed by DBU

The ring-opening reaction progress of ε-CL in the DBU-activated system at room temperature in DMSO was monitored using ^{1}H NMR and MALDI MS analysis (**Figure 5.6.**). Both *Mn* (MALDI MS) and monomer conversion (NMR) values show a relatively similar trend during the reaction. However, NMR measurements lead to significantly higher values after 1440 minutes. The difference between the values measured by the two methods can be explained by the fact that MALDI MS reflects only the CL units attached to β-CD (*Mn* measurements consider only signals for β-CDCL), while NMR measures the total amount of OCL found in the analyzed mixture as β-CDCL species and PCL homopolymers. Taking into account the differences, 7.45% of the monomer is consumed in transesterification reactions leading to the formation of cyclic

and linear PCL homopolymers. Linear homopolymers arise due to the inevitable presence of trace water when CD molecules are involved [335], whereas cyclic homopolymers result from backbiting reactions.

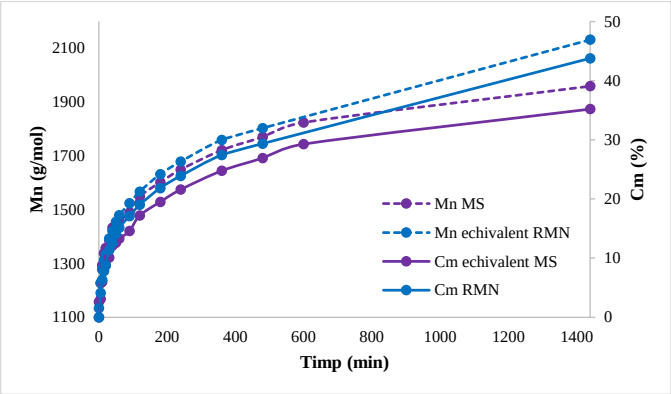

Figure 5.6. *Mn and Cm evolutions determined by MALDI MS and ^{1}H NMR for the ring-opening reaction of ε-CL organocatalyzed by DBU*

The HMBC NMR spectrum for the **β-CDCL$_{\#2}$** product (obtained after 30 min), showed acylation of the larger rim of β-CD at relatively low SD. In contrast, extending the reaction time to 24 h (**β-CDCL$_{\#3}$**) resulted in additional modifications, with an increase in the average chain length and substitution occurring at both the small and larger rims.

The substitution pattern observed in the presence of DBU can be explained by several processes. Once the lactone ring is opened and bound to positions 2 and 3, the ester groups attached to β-CD can undergo various interchange transesterification reactions. The OH groups involved in these reactions consist of the terminal oligoester functions which give chain elongation (**Scheme 5.3** – pathway 1) and backbiting (**Scheme 5.3** – pathway 3), and the primary OH groups of β-CD leading to small rim functionalization (**Scheme 5.3** – pathway 2).

The transfer toward position 6 can be explained by the geometry of the C2,3 acylated product, the OCL units being included in the β-CD cavity. ROESY experiments for **β-CDCL$_{\#2}$** revealed NOE correlation signals between Hα of OCL chains and H3/5 and OH6 of β-CD (**Figure 5.12**). The monomer units attached to the larger rim are located in the macrocycle cavity, with the CH2α in the proximity of OH6 (less than 5Å).

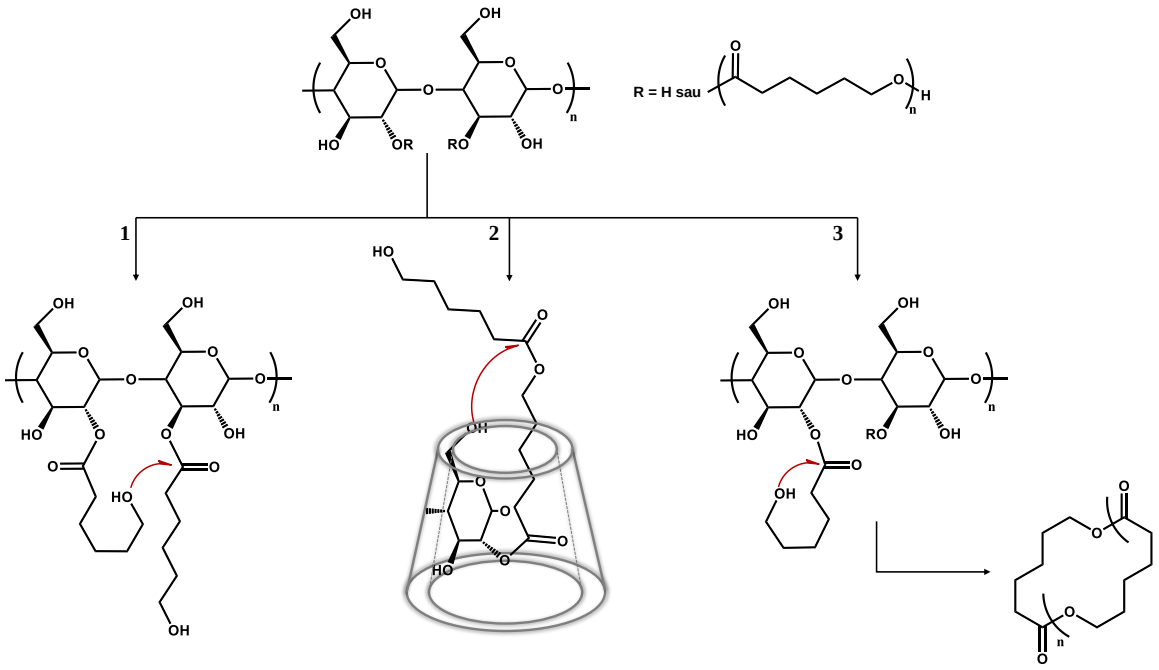

Scheme 5.3 *The transesterification pathways of a β-CDCL product substituted in positions 2 and 3: 1 - chain elongation; 2 - C2,3/C6 exchanges; 3 - backbiting*

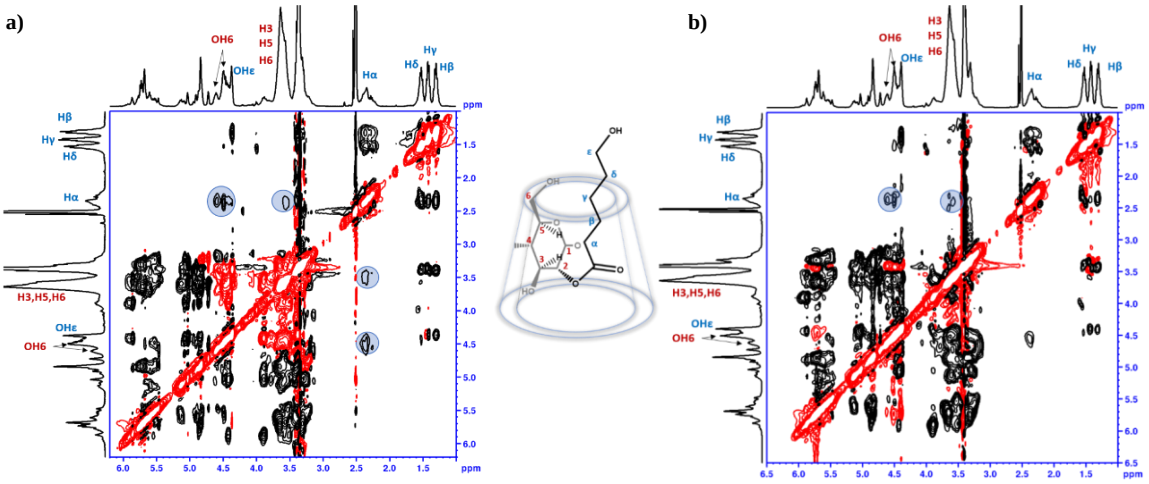

Figure 5.12. *ROESY spectra of β-CDCL$_{\#2}$ at a) 10 mM and b) 40 mM in DMSO-d6, highlighting the NOE correlation signals between OH6, H3, and H5 from β-CD and Hα from OCL and a schematic representation for the auto-inclusion of OCL chains in the β-CD cavity*

5.2.4. Comparative ^{1}H NMR and MALDI MS studies for the ROO process of ε-CL organocatalyzed of TBD

MALDI MS and NMR analyses were used to monitor changes in the ring-opening process of ε-CL catalyzed by TBD (**Figure 5.13a**). The reaction showed a two-step evolution in terms of *Mn* and ε-CL conversion values. In the first 15 min, both analytical methods gave comparable results, with similar values. From 60 to 120 minutes, MALDI MS analysis revealed

a plateau region, while NMR analysis showed a gradual increase in conversion up to 85.65%, in contrast to the equivalent conversion of 58.15% determined by MS. This significant difference can be attributed to a 27.5% ε-CL consumption in secondary transesterification reactions with the formation of PCL homopolymers. In addition, the continuous increase of Đ, even after the stagnation of *Mn*, provides further evidence for transesterification (**Figure 5.13b**). Considering the reaction kinetics of the ROO process initiated by β-CD in the presence of TBD, three β-CDCL products were isolated after 10 min (β-CDCL$_{\#4}$), 60 min (β-CDCL$_{\#5}$), and 1440 min (β-CDCL$_{\#6}$) to determine the substitution pattern.

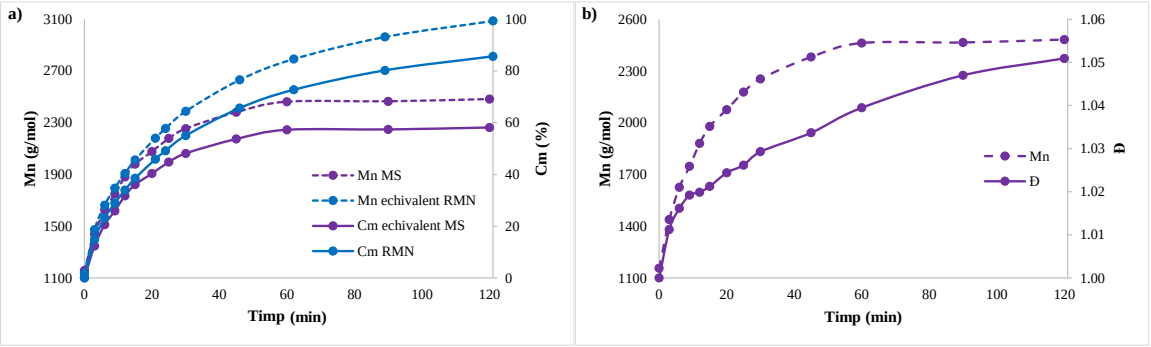

Figure 5.13. *a) Mn and Cm evolutions determined by MALDI MS and ^{1}H NMR for the ring-opening reaction of ε-CL catalyzed by TBD and b) Mn and Đ evolutions determined by MALDI MS*

The **β-CDCL$_{\#4}$** product showed a value of 6.35 CL units/β-CD, as indicated by both analytical methods, and ^{1}H NMR showed a random substitution pattern. After 60 min, a **β-CDCL$_{\#5}$** derivative was isolated, having a *Mn* value of 3050 g/mol, indicating the attachment of 16.6 CL units to the β-CD molecule. Also, the mass spectrum (**Figure 5.14**) confirms the presence of cyclic PCL (*A series*) and linear PCL (*B-D series*). NMR analysis of this product showed random substitution at positions 2, 3, and 6, having 15.42 CL units/β-CD. The presence of linear PCL homopolymers was also confirmed by the corresponding COOH signals.

The **β-CDCL$_{\#6}$** product, obtained after a reaction time of 24 h, marks a new stage in the evolution of the reaction system. Thus, when comparing the *Mn* values obtained by MALDI MS of the β-CDCL$_{\#5}$ and β-CDCL$_{\#6}$ products, a significantly lower value is obtained for the second derivative (2575 g/mol), corresponding to the attachment of 12.43 CL units/β-CD. The decreased values of *Mn* can be correlated with the detachment of the oligoester chains by transfer reactions to water molecules in the system and backbiting. On the other hand, NMR analysis of the β-CDCL$_{\#6}$ product indicates exclusive substitution at position 6.

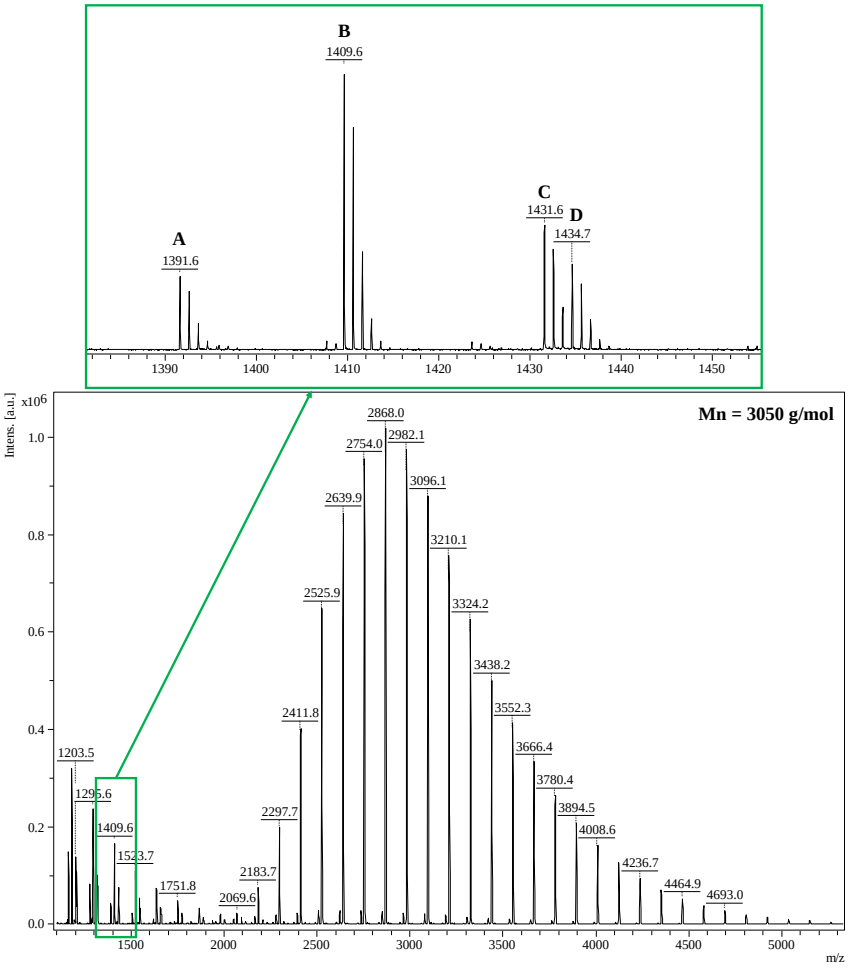

Figure 5.14 *MALDI MS spectrum of β-CDCL$_{\#5}$ with the main peak population corresponding to [β-CDCL+Na]$^+$ species and highlighting the peak series of PCL homopolymers accompanying the main product (A – cyclic PCL, B – linear PCL with COOH end chain, C – linear PCL with COONa end chain and D – linear PCL with COO–TBD end chain)*

5.2.5. Analysis of transfer reactions from positions 2 and 3 in 6

To accurately reflect the system evolution during the transfer from positions 2,3 to 6, the reaction was performed in the NMR tube (**Figure 5.22**). The^1 H NMR spectrum recorded immediately after the addition of TBD shows signals for a β-CDCL product with a low degree of functionalization and signals associated with cyclic ε-CL formed *in situ,* indicating cyclization processes.

Analysis of the collected NMR spectra over time reveals that the enhancement of the H6'a, H6'b, and H5' signals is accompanied by the disappearance of the H2' and H3' signals. This suggests a loss of functionalization at positions 2 and 3, concomitant with a transfer of functionalities to position 6. Also, the continuous decrease in the amount of ε-CL indicates the

consumption of the monomer by an irreversible process, different from the initially detected acylation/deacylation process. In addition, the 3.99 ppm signal corresponding to chain Hε increases steadily, indicating elongation of the grafted chains at position 6. Upon the transformation of β-CDCL$_{\#2}$ in **β-CDCL$_{\#8}$**, the monomer units attached at positions 2 and 3 are slowly transferred to position 6. After 7 h, the substitution at position 6 is almost exclusively detected, and the β-CDCL$_{\#8}$ product (isolated after 24 h) has longer chains compared to the original derivative, showing that the C2,3 to C6 transfer contributes to chain elongation.

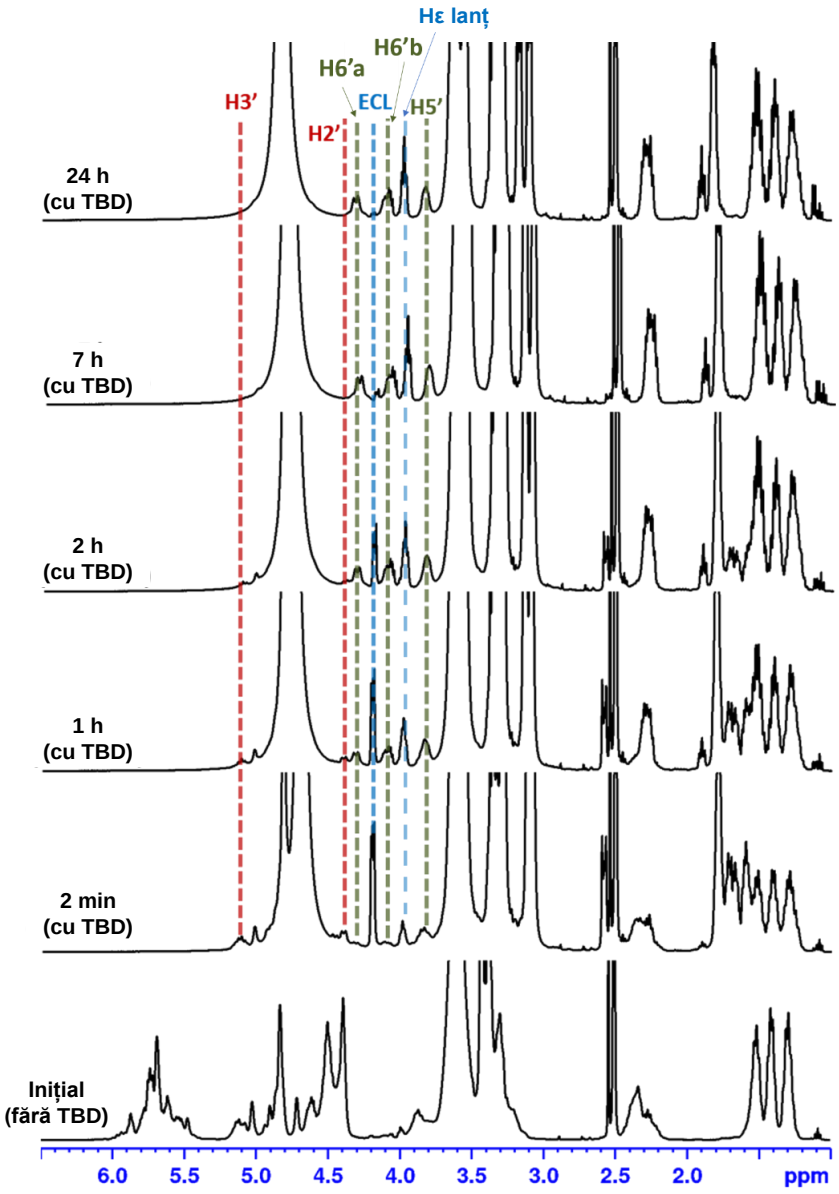

Figure 5.22. *^{1}H NMR spectra highlighting the evolution of TBD-catalyzed transesterification and showing the formation of β-CDCL$_{\#8}$ from β-CDCL$_{\#2}$*

5.2.7. Influence of α-, β-, or γ-CD in the ROO process of ε-CL - MALDI MS kinetics

The ring-opening reaction of ε-CL was monitored for 120 min to determine the influence of α-, β-, and γ-CD. Thus, the evolution of *Mn* values, respectively the average number of CL units/CD, was followed for the three systems by MALDI MS (**Figure 5.29**). The comparative data highlight that all systems show a two-step evolution of *Mn* values, very well evidenced for the α-CD-initiated reaction. The β- and γ-CD have a higher reactivity, leading faster to high SD values. Although γ-CD gives a higher SD than β-CD, the Đ values are significantly higher for the latter. Thus, it can be stated that the α-CD system was the least reactive as the monomer is stronger included in the cavity [313], while the β-CD system was the most reactive, in line with previous studies [46-48]. This indicates that complexation phenomena are at least partially involved in the ROO process of ε-CL in DMSO.

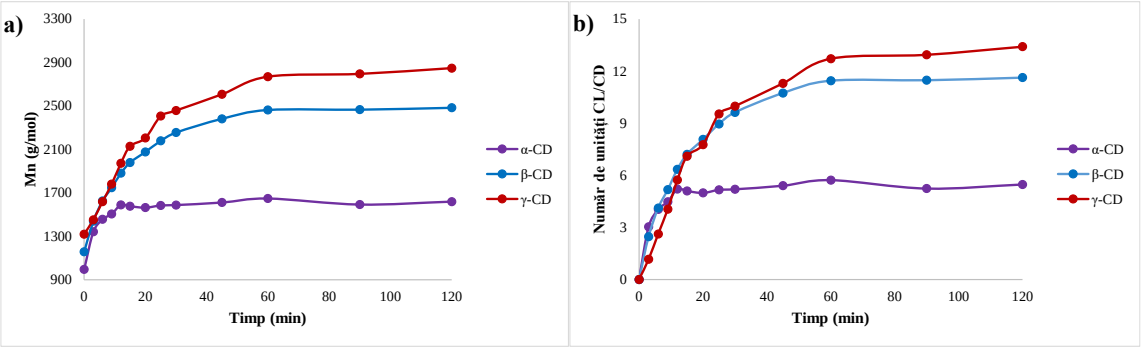

Figure 5.29. *Evolution of a) Mn values and b) the average number of CL units/CD for the ROO of ε-CL initiated by α-, β-, and γ-CD in the presence of TBD*

6. MONITORING THE CYCLODEXTRIN-OLIGOVALEROLACTONE SYNTHESIS BY MALDI MS

The β-CDVL derivatives are prepared by the ROO process of δ-VL initiated by β-CD in solution (DMSO) according to **Scheme 6.1**. The mass spectrum of a typical β-CDVL product (isolated after 5 min from a TBD-activated system) exhibits a series of peaks having 100 Da differences, corresponding to the molecular mass of the VL monomer unit, starting from the sodium adduct of β-CD (**Figure 6.1**). MS/MS fragmentation studies were also used to confirm the structure of the β-CDVL derivatives. NMR analysis also shows that the β-CD is substituted with VL units at the smaller rim.

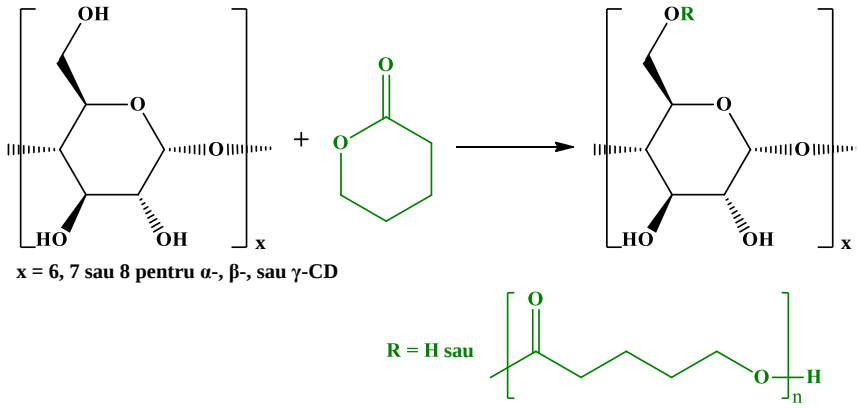

Scheme 6.1. *The ring-opening reaction of δ-VL initiated by β-CD*

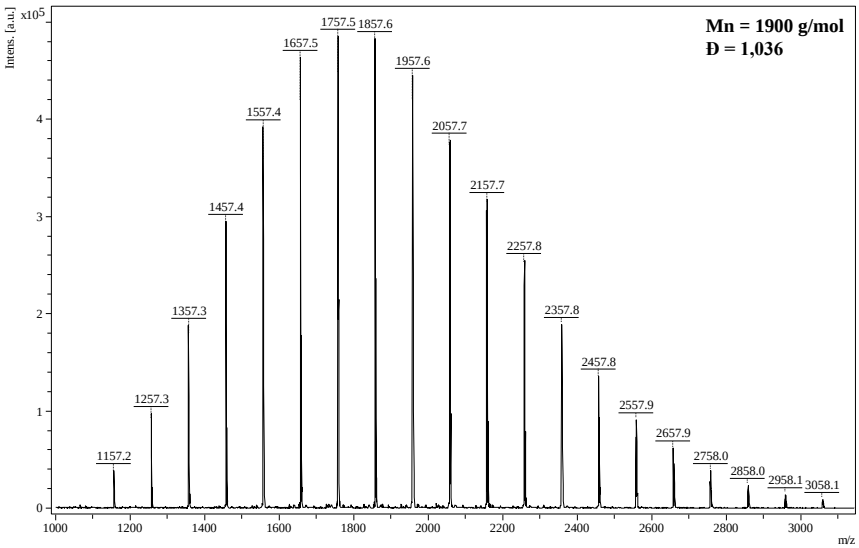

Figure 6.1. *MALDI MS spectrum of β-CDVL$_{\#3}$*

6.2.2. Ring-opening reaction of δ-VL initiated by β-CD

The evolution of the DBU-activated ROO process of the δ-VL monomer initiated by β-CD was determined by both MALDI MS and ^{1}H NMR (**Figure 6.6a**). The *Mn* evolution determined directly from MALDI MS, and indirectly, from NMR using the monomer conversion is similar, leading to the same values at the end of the reaction time. For the first 360 minutes, the reaction has a higher *Mn* increase rate, but thereafter it slows down. The reduction in reactivity can be attributed to the modification of the β-CD structure and hence, steric hindrance at the β-CD reactive sites. The Đ values increase significantly for most of the reaction time (**Figure 6.6b**), and the MALDI MS spectrum of the product obtained after 1440 min showed the presence of linear PVL homopolymers, resulting from water traces in the reaction

medium, in the 500-1100 Da region. Surprisingly, NMR analysis of the spectra recorded to determine the evolution of the ROO process reveals that the substitution occurs at the primary hydroxyl groups right from the beginning of the reaction.

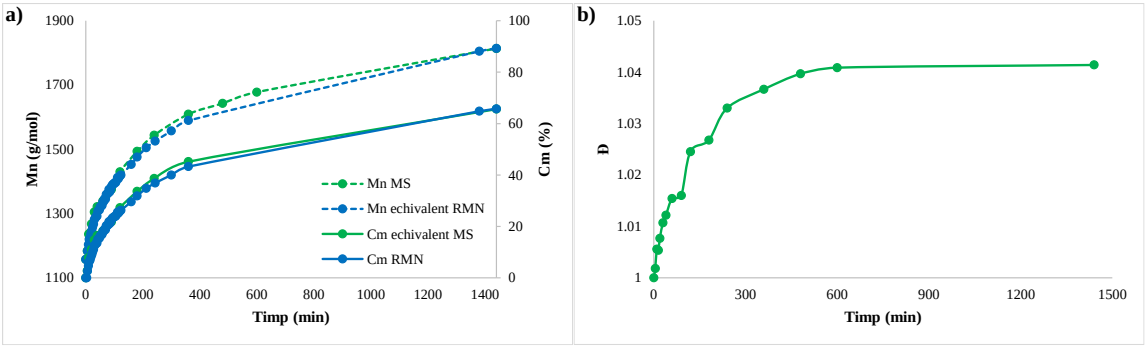

Figure 6.6. *Evolution of a) Mn (determined from MALDI MS and NMR) and b) Đ (determined from MALDI MS) in the ROO process of δ-VL catalyzed by DBU*

The DBU-catalyzed reaction led to a moderate conversion of δ-VL, so the progress of the reaction was also investigated in the presence of a stronger nucleophilic base, TBD (**Figure 6.10a**). The evolution of the reaction system in terms of *Mn* values (monitored by MALDI MS) showed a rapid increase during the first 15 min; after this initial increase, the reaction system reached a plateau region. Although *Mn* values remain relatively constant, Đ values continue to increase (**Figure 6.10b**) confirming the incidence of transesterification reactions.

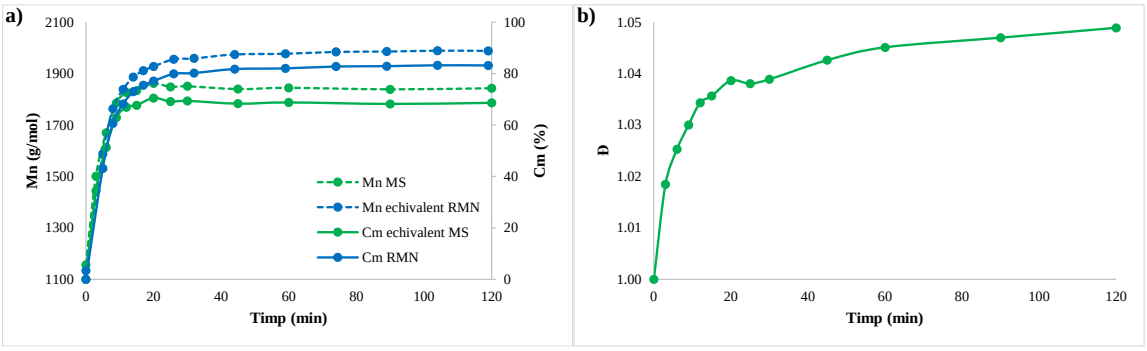

Figure 6.10 *Evolution of a) Mn (determined from MALDI MS and NMR) and b) Đ (determined from MALDI MS) in the ROO process of δ-VL catalyzed by TBD*

The reaction progress followed by NMR, based on monomer conversion converted to equivalent *Mn*, leads after 15 min to higher values than those determined by MALDI MS. However, the kinetic profiles are similar, each reaching a plateau by the end of the reaction, indicating that the ROO equilibrium has been attained under the given conditions. Also, the

differences in conversion values determined by the two analytical techniques signal that 14.35% of the monomer is converted to homopolymers. Similar to the previous case, NMR analysis reveals that substitution occurs at the primary hydroxyl groups from the very beginning of the reaction. The high reactivity of the system prevents the observation of larger rim substitution.

6.2.3. Influence of the α-, β-, or γ-CD cavity on the δ-VL ROO process

Reactions initiated by α-, β-and γ-CD were monitored for 120 minutes to assess the evolution of *Mn* values (**Figure 6.14a**) and the number of VL units attached to CD molecules, for a clearer differentiation of the three systems (**Figure 6.14b**). The very well-differentiated two-step evolution may be a consequence of the increased reactivity in the initial reaction step due to the TBD organocatalyst and the high concentration of active hydroxyl species acting as initiators. However, the theoretical maximum conversion is not reached in any of the studied cases, likely due to the attainment of a steady state in the reversible attachment and detachment of δ-VL to CD.

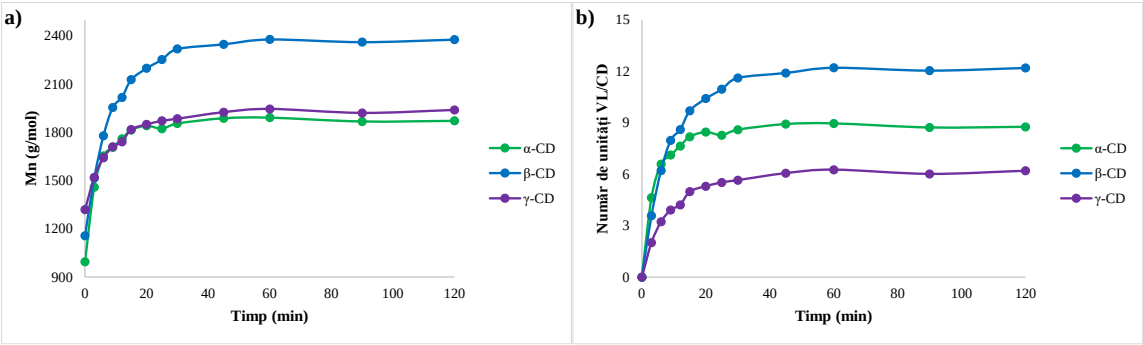

Figure 6.14. *Evolution of a) Mn values and b) number of VL units/CD for the ROO of δ-VL initiated by α-, β-, and γ-CD in the presence of TBD*

Considering only the mass increase, the α-CD-initiated system appears similar to the γ-CD system. In contrast, the α-CDVL system exhibits a higher SD of 8.2 units in the first 15 minutes. In the γ-CD-initiated reaction, the process progresses rapidly for the first 15 minutes, when 5 VL units are attached to γ-CD (**Figure 6.14b**). Following this initial increase, the growth rate slows considerably, and considering the larger size of the γ-CD cavity, respectively the inefficient immobilization of the lactone in its cavity [313], it can be assumed that the lower reactivity is the result of an inefficient complexation/activation process of δ-VL. The best results are obtained in the case of β-CD, in line with previous studies [46-48].

7. ELECTROSPINNING OF OLIGO-MODIFIED CYCLODEXTRINS

7.1. Elect electrospinning of α-, β- and γ-CDLA derivatives

Based on previous results of β-CDLA electrospinning in water/acetonitrile [42], a concentration of 160% w/v was chosen as the starting point for the preparation of CDLA nanofibers in water/ethanol. At this concentration, fibers were obtained for both β- and γ-CDLA, but in the case of α-CDLA, it was necessary to further increase the concentration up to 200% w/v to form bead-free fibers (**Figure 7.5**). The average diameter of the α- and β-CDLA nanofibers is relatively similar, 333 ± 52 nm and 378 ± 68 nm. The larger diameter of γ-CDLA nanofibers (468 ± 130 nm) can be explained by the higher viscosity of the γ-CDLA solution (0.818 Pa·s) compared to approximately 0.6 Pa·s in the case of the other derivatives.

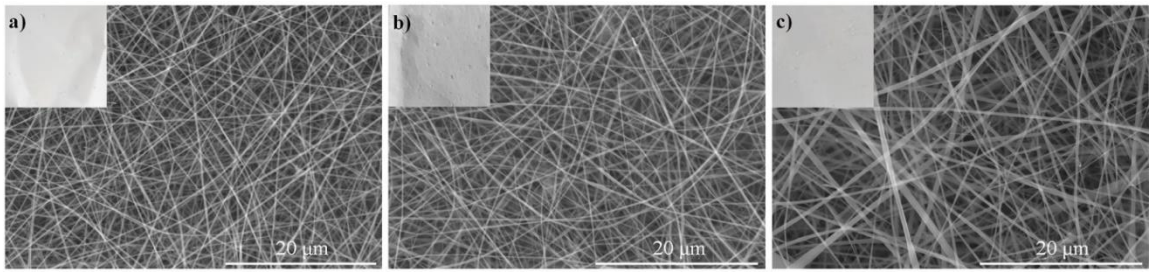

Figure 7.5. *SEM images of nanofibers based on: a) α-CDLA (200% w/v), b) β-CDLA (160% w/v), and c) γ-CDLA (160% w/v)*

7.2.2. Electrospinning process of β-CDVL and β-CDCL derivatives

In the electrospinning process, the transition from particles to beaded fibers and finally to bead-free fibers occurs with increasing concentration and/or viscosity of the solution [228]. Varying the concentration range from 110% to 200% w/v (**Figure 7.9**) highlights the tendency towards fiber formation for β-CDCL in DMF. At 110%, only particles are observed (**Figure 7.9a**) and higher concentrations result in the simultaneous formation of both fibers and particles (**Figure 7.9b-d**). At concentrations of 190% and 200% w/v, β-CDCL fibers are formed without particles, with mean diameters of 632 ± 188 nm and 862 ± 311 nm, respectively (**Figure 7.9e**,**f**).

Based on the results obtained from the electrospinning of β-CDLA [42] and β-CDCL derivatives, the initial concentration tested for the β-CDVL solution was 150% w/v in DMF. At this concentration, β-CDVL derivatives resulted in particle formation (**Figure 7.11a**), indicating that a higher concentration is necessary to achieve the level of hydrogen bond cohesion required for fiber formation. Increasing the concentration to 210% w/v yielded fibers with a few elongated particles, the fibers having an average diameter of 1098 ± 477 nm (**Figure 7.11d**).

Thus, the concentration was increased to 220% w/v to reduce the presence of particles (**Figure 7.11e**). The resulting average fiber diameter was quite large (1108 ± 312 nm), and to reduce the diameter, the needle-to-collector distance was increased during the electrospinning of the 220% m/v solution, which led to a decreased average fiber diameter of 629 ± 123 nm (**Figure 7.11f**).

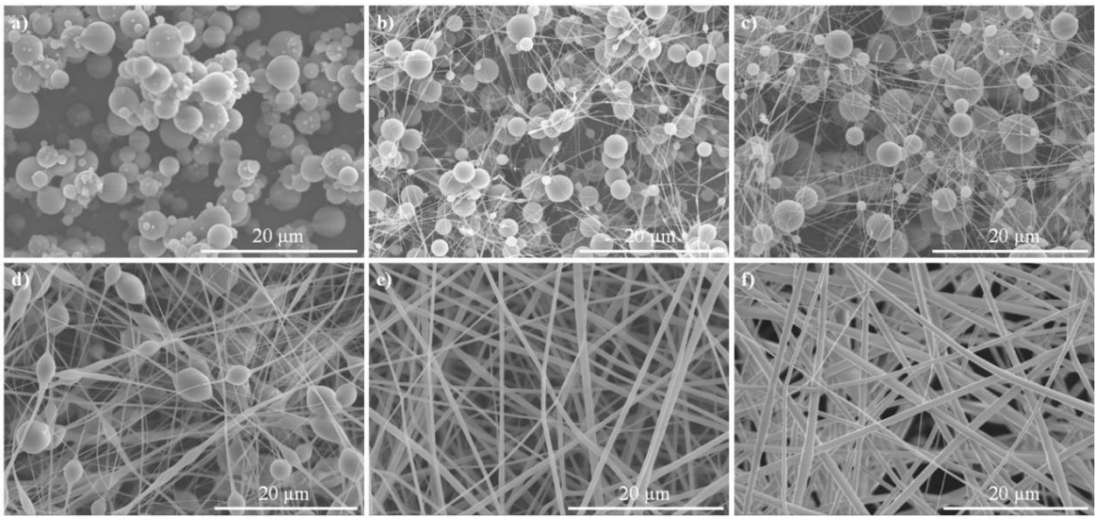

Figure 7.9. *SEM images for β-CDCL systems at a) 110% w/v, b) 130% w/v, c) 150% w/v, d) 170% w/v, e) 190% w/v and f) 200% w/v*

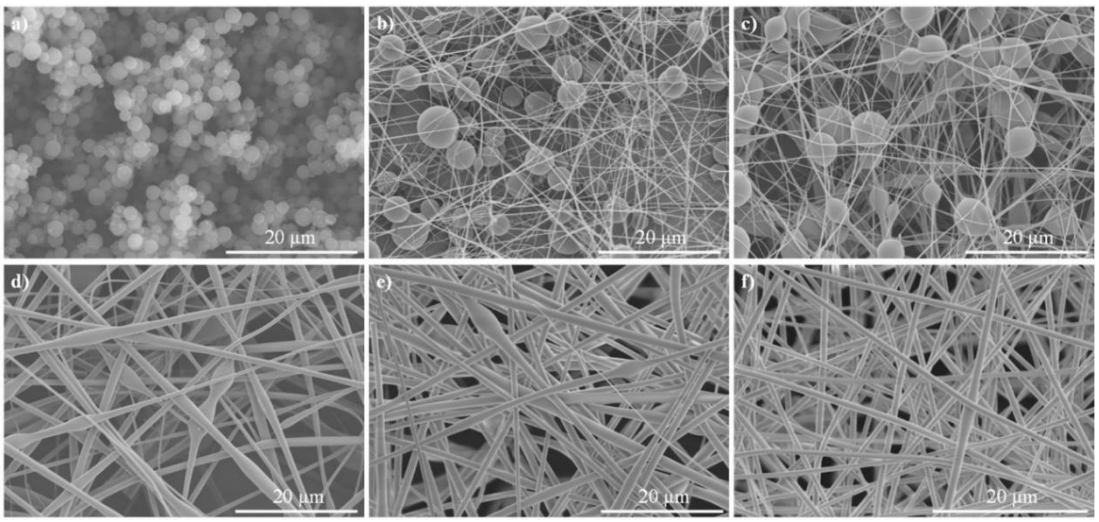

Figure 7.11. *SEM images for β-CDVL systems at a) 150% m/v, b) 170% m/v, c) 190% m/v, d) 210% m/v, e) 220% m/v at 15 cm, f) 220% m/v at 18 cm needle-to-collector distance*

7.3. Electrospinning of cyclodextrin-oligolactide derivatives with active principles

7.3.1. Curcumin nanofibers

Increasing the concentration of β-CDLA solution to 180% w/v (for a molar ratio of 4/1 β-CDLA/CRC), resulted in nanofiber formation, with a diameter of 302 ± 55 nm (**Figure 7.14b**).

The γ-CDLA/CRC system led to nanofibers under the same conditions as β-CDLA/CRC, with an average diameter of 408 ± 104 nm (**Figure 7.14c**). On the other hand, a higher concentration was required to obtain nanofibers from the α-CDLA system with CRC (220% w/v α-CDLA for an α-CDLA/CRC molar ratio of 4/1). The SEM image reveals the formation of nanofibers from the α-CDLA/CRC system with an average diameter of 264 ± 44 nm (**Figure 7.14a**).

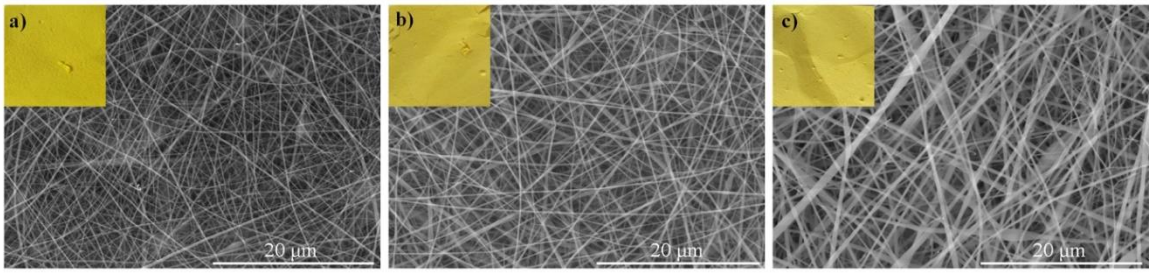

Figure 7.14. *SEM images for a) α-CDLA/CRC (220% m/v), b) β-CDLA/CRC (180% m/v), and c) γ-CDLA/CRC (180% m/v)*

7.3.1.3. Antioxidant activity of α-, β-, and γ-CDLA/curcumin nanofibers

The β- and γ-CDLA nanofibers loaded with CRC exhibited similar performances (74.3% vs. 75.5% antioxidant activity), with a minor improvement observed for γ-CDLA nanofibers, almost similar to the pure CRC content (**Figure 7.26**).

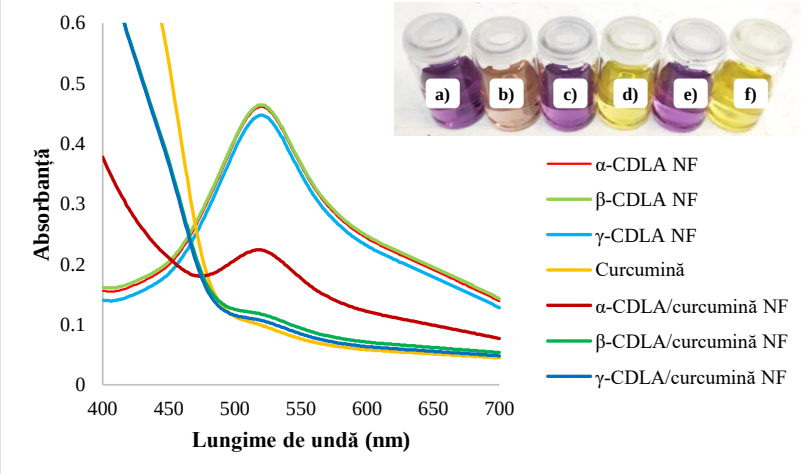

Figure 7.26. *UV-Vis spectra of the sample solutions showing the DPPH antioxidant performance of pristine and CRC-loaded α-, β- and γ-CDLA nanofibers (NF)*

In contrast, α-CDLA nanofibers demonstrated significantly lower performance, with only 51.3% antioxidant activity. This reduced effectiveness is likely due to the lower solubilization

capacity of CRC in aqueous solutions. This finding aligns with previous analyses by DTG and FTIR, which indicated less efficient host-guest interactions in α-CDLA/CRC nanofibers.

7.3.2. Magnolol and honokiol nanofibers

Nanofibers based on β-CDLA with MG and HK were prepared using solutions of 180% w/v in water/acetonitrile mixture (1/1 volume ratio) and a β-CDLA/compound molar ratio of 1/1, the compound mass content being about 7%. Under these conditions, the electrospinning of the β-CDLA/MG solution produced fibers with diameters of 416 ± 125 nm (**Figure 7.27b**), while the β-CDLA/HK system yielded fibers with diameters of 446 ± 111 nm (**Figure 7.27c**). Pristine β-CDLA fibers were also prepared, having diameters of 374 ± 115 nm (**Figure 7.27a**).

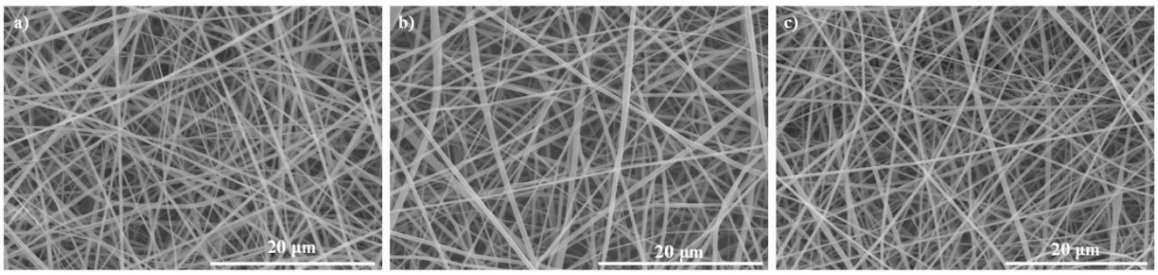

Figure 7.27. *SEM images for a) β-CDLA, b) β-CDLA/MG, c) β-CDLA/HK at 180% w/v*

7.3.2.3. Antioxidant activity of β-CDLA nanofibers with magnolol and honokiol

This study investigates the antioxidant activity of β-CDLA/MG and β-CDLA/HK nanofiber formulations (**Figure 7.33**). Over 120 min, HK and MG exhibited higher antioxidant activities than the corresponding β-CDLA formulations. This may be a consequence of the interaction between the bioactive compounds and β-CDLA derivatives, which could hinder H donation to DPPH radicals because of steric hindrance.

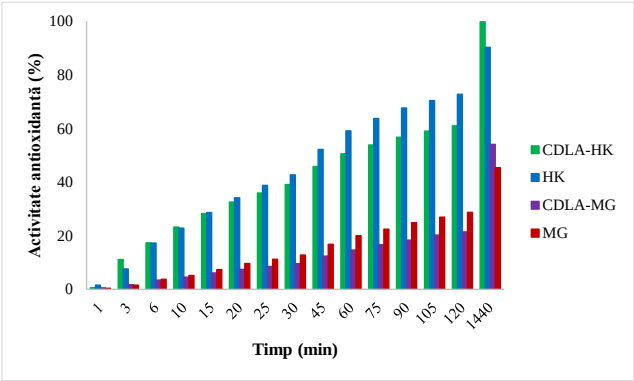

Figure 7.33. *Evolution of the antioxidant activity of β-CDLA/HK and β-CDLA/MG fiber formulations, pure HK and MG*

However, after 1440 min, the antioxidant activity values are higher for the electrospun formulations. Despite the initially slow kinetics of DPPH scavenging capacity, the β-CDLA/HK formulation reaches its maximum antioxidant activity. Similarly, the β-CDLA/MG formulation shows a slightly higher antioxidant activity compared to MG alone. Thus, interactions between the bioactive compounds and β-CDLA derivatives may enhance antioxidant activity over time.

For the β-CDLA/HK and MG nanofiber formulations, the antioxidant activity was also studied as a function of concentration in the range of 27.75-222 μg/mL after 1440 min (**Figure 7.34**). Therefore, the effective concentration (EC50) values could be determined: 31 μg/mL for β-CDLA/HK electrospun formulation and 106 μg/mL for β-CDLA/MG. The lower EC50 value indicates a higher free radical scavenging capacity for β-CDLA/HK fibers, confirming that HK exhibits significantly greater antioxidant activity compared to MG.

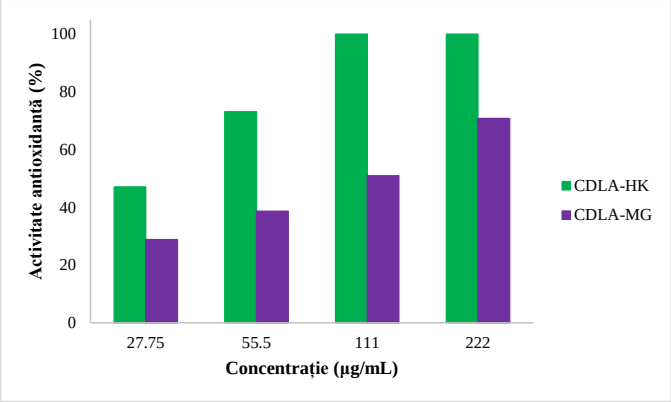

Figure 7.34. *Antioxidant activity of β-CDLA/HK and β-CDLA/MG nanofiber formulations as a function of concentration*

7.3.3. Nanofibers with enrofloxacin

Highly concentrated solutions prepared in a water/acetonitrile mixture (1/1 volume ratio) were used for the electrospinning of β-CDLA derivatives with ENR. Based on the previous results related to the electrospinning of β-CDLA derivatives with MG and HK, a 180% w/v solution was initially tested, to which an amount of active principle corresponding to a molar ratio of 1/1 β-CDLA to ENR was added. The presence of ENR in the mixture led in this case to particle formation (**Figure 7.35a**). Further increasing the concentration to 220% w/v resulted in the formation of fibers with an average diameter of 342 ± 59 nm (**Figure 7.35c**). Using a molar ratio of 2/1 β-CDLA/ENR at the same concentration, the fibers had an average diameter of 377

± 92 nm (**Figure 7.35d**). Pristine β-CDLA nanofibers were also prepared from a 220% w/v solution, having average diameters of 307 ± 77 nm (**Figure 7.35d**).

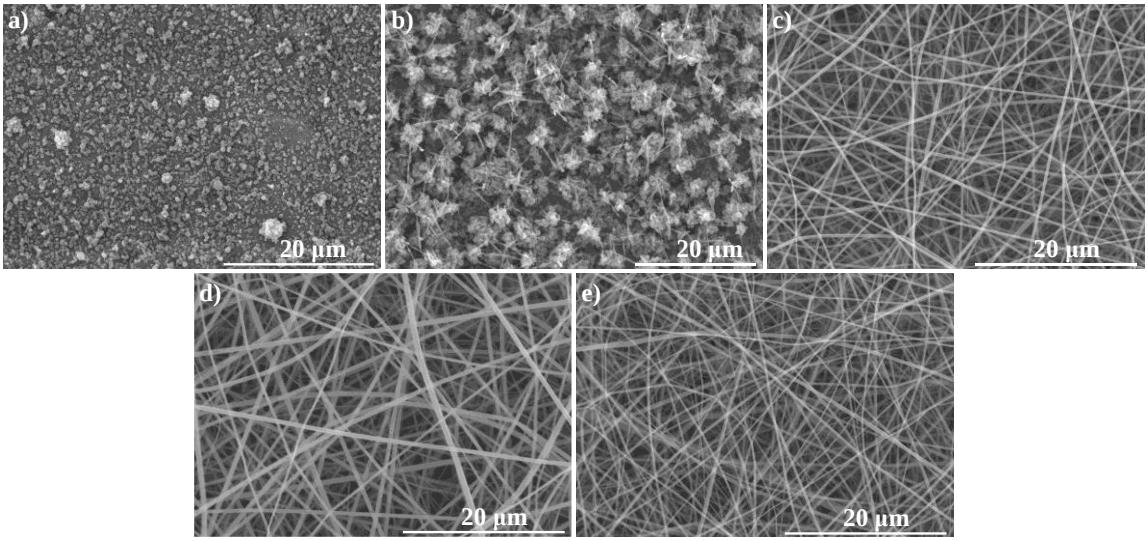

Figure 7.35. *SEM images for β-CDLA/ENR at concentrations: a) 180% w/v, b) 200% w/v, c) 220% w/v using a 1/1 β-CDLA/ENR molar ratio, d) d) 220% w/v using a molar ratio of 2/1 and e) β-CDLA 220% w/v*

7.3.3.3.Antibacterial activity of β-CDLA nanofibers with enrofloxacin

The antibacterial activity of β-CDLA/ENR nanofiber formulations was performed by disk diffusion assay using both Gram-positive (*Staphylococcus aureus*) and Gram-negative (*Escherichia coli*, *Pseudomonas aeruginosa*) bacteria. The ENR content in each sample was similar. The inhibition diameter for each tested sample (expressed in mm) is given in **Table 7.2**.

Table 7.2. *In vitro antibacterial activity of β-CDLA/ENR nanofibers*

Sample	**Inhibition diameter (mm)**		
	S. aureus	*E. coli*	*P. aeruginosa*
β-CDLA/ENR 1/1	26.1± 0.05	31.7± 0.06	17.1± 0.05
β-CDLA/ENR 2/1	27.0± 0.00	35.1± 0.05	18.0± 0.00
β-CDLA	0	15.0± 0.00	0
ENR	29.0± 0.00	34.1± 0.05	21.0± 0.00
water/DMSO (3/1 *v/v*)	0	0	0
Ciprofloxacin	26.7± 0.06	31.0± 0.00	32.3± 0.57

In general, β-CDLA/ENR formulations containing relatively high amounts of the active principle (15.6% for a molar ratio of 1/1 and 7.8% for a molar ratio of 2/1) do not significantly

affect antibacterial activity. The inhibition diameters had close values to those of pure ENR and ciprofloxacin, except for *P. aeruginosa*, where ciprofloxacin showed superior efficacy. The antibacterial activity of the nanofiber formulations can be attributed to the high concentration of the antibiotic, leading to the determined inhibition efficiency.

GENERAL CONCLUSIONS

The present thesis highlights the benefits of employing advanced structural characterization methods, specifically mass spectrometry supported by NMR spectroscopy, to better understand the mechanisms of ROO reactions in the presence of CD. The complexity of CDOE derivatives arises from various factors introduced by functionalization, including the degree of substitution, the formation of positional isomers due to multiple hydroxyl groups acting as initiators, and substitution with oligomer chains of varying lengths. The presented research addresses these challenges by adapting the MALDI MS characterization technique, both qualitatively and quantitatively, and validating the results by NMR spectroscopy.

In this context, the performed experiments were focused on the qualitative and quantitative investigation of the solution polymerization of LA, ε-CL, and δ-VL in the presence of CD, as follows:

- The synthesis of β-CDLA derivatives was monitored using an optimized MALDI MS method, validated through NMR spectroscopy, demonstrating an excellent correlation between the two techniques (**Chapter 2**). Reaction kinetics were assessed via MALDI MS by tracking changes in *Mn* values of the β-CDLA species and through ^{1}H NMR by measuring the overall monomer conversion. This kinetic analysis is important for understanding and optimizing the ROO process of cyclic esters. Mass spectrometry provided insights into the types of reactions involved in the ROO process of LA, enabling the optimization of synthesis conditions and reduction of side reactions by adjusting the reaction time, solvent type, molar ratio, or concentration. NMR analysis of a typical β-CDLA product indicated that the substitution occurs at several hydroxyl groups in position 6 of β-CD, similar to reactions conducted in bulk. Additionally, MALDI MS and MS/MS characterization revealed solvent (DMF or NMP) degradation through amide bond cleavage, leading to the formation of amines and secondary products, such as β-CDLA-formate derivatives when DMF was used.

• MALDI MS spectra provide important information for developing a method to quantify transesterification reactions in β-CDLA derivatives (**Chapter 3**). The transesterification degree can be determined using the two main types of peak series in the mass spectra. Thus, the transesterification degree was evaluated in different reaction systems to establish the influence of some parameters, particularly the addition of organocatalysts. The effect of organocatalysts on transesterification reactions was analyzed both in ROO systems and post-polymerization degradation on a β-CDLA product. The results showed that organocatalysts promote transesterifications in the following order: imidazole < DMAP < (-)-sparteine. Solvent studies indicated that DMF exhibited the highest reactivity, followed by NMP, while DMSO resulted in the lowest transesterification degree. Additionally, analysis of concentration effects revealed a higher prevalence of intramolecular transesterification reactions.

• The investigation of ROO reactions in the presence of CD also included another cyclic ester commonly used in polyester syntheses, namely ε-CL (**Chapter 4**). The kinetic data obtained from MALDI MS were in good agreement with those derived from monomer conversion using NMR analysis. Solvent effects revealed that DMF systems exhibit higher reactivity due to amide bond cleavage and the formation of dimethylamine as an activator, similar to the ROO process of LA. MALDI MS kinetic studies facilitated the identification and quantification of degradative processes, particularly when using the (-)-sparteine organocatalyst. NMR analyses led to the identification, for the first time, of two phases in the β-CD modification by ROO of ε-CL: a rapid attachment of ε-CL to secondary hydroxyl groups followed by a slower attachment to primary ones, resulting in randomly substituted derivatives. Additionally, NMR analysis allowed the identification of β-CD functionalization at the larger rim in positions 2 and 3 of the glycosidic ring.

• Building on the results obtained with amines having moderate activity such as DMAP, the experiments focused on the combined impact of β-CD and more active organocatalysts, like DBU or TBD. Specifically, the reaction kinetics and the substitution patterns of β-CDCL derivatives were studied using NMR and MALDI MS (**Chapter 5**). In the first step, it was demonstrated that an inclusion complex between β-CD and ε-CL can form in a DMSO solution. This complex plays a key role in the reaction mechanism by directing the initial substitution towards positions 2 and 3 of β-CD. This study, performed for the first time on organic solvent solutions according to literature data, demonstrates that despite the solvation effect of the CD

cavity exerted by DMSO, the monomer is included in the cavity in a geometry that enhances the proximity between the secondary hydroxyl groups at position 2 of the glycosidic ring and the ester function of ε-CL. The addition of DBU to the system maintained the selectivity for substitution at positions 2 and 3 of β-CD until a certain degree of substitution was achieved, according to the kinetic data. However, extended reaction times led to transfer reactions from positions 2 and 3 to position 6. The introduction of an even stronger organocatalyst, TBD, resulted in rapid, random substitution from the beginning of the reaction. Extending the reaction time enabled the formation of a derivative substituted exclusively at the smaller rim. Transfer reactions from positions 2 and 3 to 6 occurred through transesterification of OCL chains included in the CD cavity, as indicated by ROESY NMR data. Additionally, the TBD system led to the formation of cyclic and linear PCL, which were identified and quantified by comparing MALDI MS and NMR data. The transfer process from positions 2 and 3 to 6 was demonstrated by monitoring changes in the substitution pattern during a transesterification reaction in the presence of TBD. Starting with a product exclusively substituted at the secondary hydroxyl groups (obtained with DBU), a product substituted exclusively at position 6 was obtained after 24 h. Additionally, MALDI MS was used to evaluate the reactivity of different CDs in the ring-opening of ε-CL, establishing the following reactivity order: α-CD < γ-CD < β-CD.

- The activation of cyclic esters by CD in the presence of DBU and TBD organocatalysts was also studied for δ-VL (**Chapter 6**). Using NMR spectroscopy and MALDI MS, the kinetics of these reactions were determined, and the structures of the products were established. NMR analysis revealed that VL units are attached to the glucopyranose units of β-CD, specifically at the primary hydroxyl groups, in both systems. This substitution pattern was attributed to the higher reactivity of δ-VL compared to ε-CL (**Chapter 5**). The ROO process of δ-VL in the absence of organocatalysts resulted in exclusive substitution at positions 2 and 3, confirming a reaction mechanism similar to that proposed for ε-CL. The CD type used in the ROO of δ-VL had a significant impact on the reaction and the resulting structures, with MALDI MS kinetics establishing the following reactivity order: γ-CD < α-CD < β-CD.

- The applicative potential of CDOE derivatives (obtained from ROO processes of LA, ε-CL, and δ-VL using organocatalysts such as DMAP or TBD) was assessed by investigating their ability to form nanofibers through electrospinning without the addition of polymers (**Chapter 7**). This process takes advantage of the high solubility of CDOE derivatives compared to native

CDs to prepare the highly concentrated solutions necessary for electrospinning. Initially, electrospinning experiments were performed using concentrated solutions of α-, β-, and γ-CDLAs in low-toxicity solvent mixtures, namely water/ethanol. Nanofibers based on β- and γ-CDLA were successfully obtained at a concentration of 160% w/v, while α-CDLA required a higher concentration of 200% w/v. The resulting fiber diameters were approximately 350 nm for α- and β-CDLA, and 450 nm for γ-CDLA. Dynamic water vapor sorption studies revealed that, while β-CDLA nanofibers exhibited a higher water sorption capacity, they required a longer time to reach equilibrium compared to the corresponding powder, due to different intermolecular interactions. The β-CDCL and β-CDVL derivatives were also electrospun from concentrated solutions in DMF. β-CDCL fibers were successfully formed at a concentration of 190% m/v, while β-CDVL required a concentration exceeding 210% m/v. In both cases, the fiber diameters were approximately 630 nm. By correlating viscosity with solution concentration, the critical electrospinning concentration for both derivatives was determined, and compared with SEM results. Additionally, the study demonstrated the potential of CDLA derivatives for preparing pharmaceutical formulations of active principles (curcumin, magnolol, honokiol, and enrofloxacin) by electrospinning. Except for the α-CDLA/curcumin and β-CDLA/enrofloxacin formulations, which required concentrations of 220% w/v, all other nanofibers were successfully produced at a solution concentration of 180% w/v. The average fiber diameters varied depending on the system, ranging from 250 to 450 nm, and were correlated with the solution viscosity. The characterization techniques confirmed the presence of active principles in the nanofibers, the molar ratios between components being maintained. The antioxidant assay revealed that certain formulations exhibited superior activity, and the antibacterial evaluation demonstrated that the enrofloxacin-loaded nanofibers retained their inhibitory effectiveness.

The original results, summarized above, have been published in 6 ISI scientific papers (with a cumulative impact factor of 34.4) and presented in 9 communications and 4 posters at national and international conferences.

DISSEMINATION OF RESULTS AND OTHER SCIENTIFIC ACTIVITIES

Papers published in ISI-listed scientific journals (results included in the thesis)

1. **Blaj D.-A.**, Peptu C.A., Danu M., Harabagiu V., Peptu C., Bujor A., Ochiuz L., Tuchiluș C.G. Enrofloxacin Pharmaceutical Formulations through the Polymer-Free

Electrospinning of β-Cyclodextrin-oligolactide Derivatives, Pharmaceutics, 16, 903, 2024. (FI: 4.9)

2. **Blaj D.-A.**, Balan-Porcarasu M., Harabagiu V., Peptu C. Synthesis of β-cyclodextrin derivatives substituted at larger or smaller rims via amine-catalyzed ring-opening oligomerization of ε-caprolactone, Carbohydrate Polymers, 334, 122032, 2024. (FI: 10.7)
3. Peptu C., **Blaj, D.-A.**, Balan-Porcarasu M., Peptu C.A., Harabagiu V. Custom-modified oligolactide-cyclodextrin derivatives for electrospun drug formulations. European Polymer Journal, 196, 112234, 2023. (FI: 5.8)
4. **Blaj D.-A.**, Kowalczuk M., Peptu C. Mass Spectrometry of Esterified Cyclodextrins. Molecules, 28, 2001, 2023. (FI: 4.2)
5. Peptu C., **Blaj D.-A.**, Balan-Porcarasu M., Rydz J. Cyclodextrin-Oligocaprolactone Derivatives-Synthesis and Advanced Structural Characterization by MALDI Mass Spectrometry. Polymers, 14, 1436, 2022. (FI: 4.7)
6. **Blaj D.A. Blaj**, Balan-Porcarasu M., Petre B.A., Harabagiu V., Peptu C. MALDI mass spectrometry monitoring of cyclodextrin-oligolactide derivatives synthesis. Polymer, 233, 124186, 2021 (ISI FI: 4.1)

Papers published in ISI-listed scientific journals (results not included in the thesis)

1. **Blaj D.-A.**, Diaconu A.-D., Harabagiu V., Peptu C. Polyethylene Glycol-Isophorone Diisocyanate Polyurethane Prepolymers Tailored Using MALDI MS. Materials, 16, 821, 2023. (FI: 3.1)
2. Damoc M., Stoica A.-C., **Blaj D.-A.**, Macsim A.-M., Dascalu M., Cojocaru C., Shova S., Cazacu M. Fourteen-member silacycle built by cascade reactions induced by a platinum catalyst, Journal of Molecular Structure, 1269, 133760, 2022. (FI: 4)

Book chapter (not included in the thesis)

1. **Blaj D.-A.**, Rotaru R., Peptu C. 16 - Protective textiles from natural resources for electromagnetic shielding, Editor(s): Md. Ibrahim H. Mondal, In The Textile Institute Book Series, Protective Textiles from Natural Resources, Woodhead Publishing, 2022, Pages 469-510, ISBN 9780323904773.

Participation in national and international scientific events (results included in thesis)

a. Oral communications

1. MALDI MS Kinetics for Ring-Opening Oligomerization of Cyclic Esters in the Presence of Cyclodextrin, Cristian Peptu, **Diana-Andreea Blaj**, Mihaela Balan-Porcarasu, 40th Informal Meeting on Mass Spectrometry, 12-15 May 2024, Budapest, Hungary.
2. MALDI mass spectrometry mass spectrometry-based analytical approach for the analysis of ring-opening oligomerization of cyclic esters in the presence of cyclodextrin, Cristian Peptu, **Diana-Andreea Blaj**, Mihaela Balan-Porcarasu, Valeria Harabagiu, 29th edition of Progress in the Science of Organic and Macromolecular Compounds, 4-6 October 2023, Iași, Romania.
3. The influence of cyclodextrin's cavity size on the ring-opening oligomerization of cyclic esters, **Diana-Andreea Blaj**, Valeria Harabagiu, Cristian Peptu, 33rd edition of the International Conference of "Apollonia" University, 2-5 March 2023, Iași, Romania.
4. Reactivity insights in β-cyclodextrin-ε-caprolactone oligomerization reactions by MALDI mass spectrometry, **D. A. Blaj**, M. Balan-Porcarasu, V. Harabagiu, C. Peptu, 3rd edition of Scientific communications session of young researchers (MacroYouth 2022), November 18, 2022, Iași, Romania.
5. NMR study of some β-cyclodextrin-oligocaprolactone derivatives, M. Balan-Porcarasu, **D. A. Blaj**, C. Peptu, V. Harabagiu, 3rd edition of Scientific communications session of young researchers (MacroYouth 2022), November 18, 2022, Iași, Romania.
6. Cyclodextrin initiated ring opening oligomerization of ε-caprolactone - structural insights via MALDI mass spectrometry and NMR spectroscopy, **D. A. Blaj**, M. Balan-Porcarasu, V. Harabagiu, C. Peptu, 32nd edition of the International Conference of "Apollonia" University, 1-2 March 2022, Iași, Romania.
7. Elucidation of Complex Structures through Mass Spectrometry Fragmentation Studies, **D. A. Blaj**, M. Balan-Porcarasu, V. Harabagiu, C. Peptu, 2nd edition of Scientific communications session of young researchers (MacroYouth 2021), November 19, 2021, Iași, Romania.
8. Mass Spectrometry Monitoring of Polymerization Reactions in the Presence of Cyclodextrins, **D. Blaj**, V. Harabagiu, C. Peptu, 1st edition of Scientific communications session of young researchers (MacroYouth 2020), November 19, 2020, Iași, Romania.

9. MALDI mass spectrometry as a tool for the structural characterization of the complex chemical structures, **D. Blaj**, C. Peptu, 30th edition of the International Conference of "Apollonia" University, February 28 - March 3, 2020, Iași, Romania.

b. Posters

1. MALDI MS Quantification of Transesterification Reactions in the Ring-Opening Polymerization of Lactides, **Diana-Andreea Blaj**, Cristian Peptu, 40th Informal Meeting on Mass Spectrometry, 12-15 May 2024, Budapest, Hungary.
2. MALDI mass spectrometry monitoring of cyclodextrin-oligolactide synthesis, **D.-A. Blaj**, C. Peptu, V. Harabagiu, The Silesian Meetings on Polymer Materials POLYMAT 2022 - March 17, 2022, Zabrze, Poland.
3. Cyclodextrin-oligocaprolactone synthesis - advanced structural studies by MALDI mass spectrometry and NMR spectroscopy, C. Peptu, **D.-A. Blaj**, M. Balan-Porcarasu, J. Rydz, The Silesian Meetings on Polymer Materials POLYMAT 2022, March 17, 2022, Zabrze, Poland.
4. Cyclodextrin involvement in the ring opening polymerization of D,L-lactide monitored by MALDI mass spectrometry, **D. Blaj**, C. Peptu, V. Harabagiu, 4th International EPNOE Junior Scientist Meeting, February 3-4, 2021.

Member of the research teams of the projects

1. Dynamic platforms based on oligo/polysaccharide cross-linked by thiol-ene reactions with biomedical applications, project **PN-III-P4-PCE-2021-1365**, funding contract no. PCE115/2022 (2022-2024).
2. *Design of cyclodextrin-polyester-amides for special applications* (Project of Inter-Academic Exchanges between the Romanian Academy (ICMPP, Iași) and the Polish Academy of Sciences (Center of Polymer and Carbon Materials Polish Academy of Sciences, Zabrze).
3. *PHA-based inclusion complexes with cyclodextrin - preparation and degradation study* (Project of Inter-Academic Exchanges between the Romanian Academy (ICMPP, Iași) and the Polish Academy of Sciences (Center of Polymer and Carbon Materials Polish Academy of Sciences, Zabrze).

REFERENCES

Crini G. A History of Cyclodextrins. Chemical Reviews, 114(21), 10940-10975, 2014.

Topuz F., Uyar T. Electrospinning of Cyclodextrin Functional Nanofibers for Drug Delivery Applications.Pharmaceutics, 11(6), 6, 2019.

Shen Z., Hai A., Du G., Zhang H., Sun H. A convenient preparation of 6-oligo(lactic acid)cyclomaltoheptaose as kinetically degradable derivative for controlled release of amoxicillin. Carbohydrate Research, 343, 2517-2522, 2008.

Opalkova Siskova A., Sacarescu L., Opalek A., Mosnacek J., Peptu C. Electrospinning of Cyclodextrin-Oligolactide Derivatives. Biomolecules, 13, 203, 2023.

Takashima Y., Osaki M., Harada A. Cyclodextrin-Initiated Polymerization of Cyclic Esters in Bulk: Formation of Polyester-Tethered Cyclodextrins. Journal of the American Chemical Society, 126, 13588-13589, 2004.

Weidner S.M., Kricheldorf H.R. Transesterification in the solid state of cyclic and linear poly(L-lactide)s. Macromolecular Chemistry and Physics, 218, 1700114, 2017.

Dove A. Organic catalysis for ring-opening polymerization. ACS Macro Letters, 1, 1409-1412, 2012.

Nederberg N., Connor E.F., Moller M., Glauser T., Hedrick J.L. New paradigms for organic catalysts: the first organocatalytic living polymerization. Angewandte Chemie International Edition, 40, 2712-2715, 2001.

Coulembier O., Dubois P. 4-dimethylaminopyridine-based organoactivation: from simple esterification to lactide ring-opening "Living" polymerization. Journal of Polymer Science Part A: Polymer Chemistry, 50, 1672-1680, 2012.

Lohmeijer B.G.C., Pratt R.C., Leibfarth F., Logan J.W., Long D.A., Dove A.P., Nederberg F., Choi J., Wade C., Waymouth R.M., Hedrick J.L. Guanidine and amidine organocatalysts for ring-opening polymerization of cyclic esters. Macromolecules, 39, 8574-8583, 2006.

Coulembier O., Josse T., Guillerm B., Gerbaux P., Dubois P. An imidazole-based organocatalyst designed for bulk polymerization of lactide isomers: inspiration from Nature. Chemical Communications, 48, 11695-11697, 2012.

Coulembier O., de Winter J., Josse T., Mespouille L., Gerbaux P., Dubois P. One-step synthesis of polylactide macrocycles from sparteine-initiated ROP. Polymer Chemistry, 5, 2103, 2014.

Weidner S.M., Kricheldorf H.R. Transesterification in alcohol-initiated ROPs of L- and meso-lactide catalyzed by Sn(II) and Sn(IV) compounds at low temperatures. Macromolecular Chemistry and Physics, 1800445, 2018.

Peptu C., Nicolescu A., Peptu C.A., Harabagiu V., Simionescu B.C., Kowalczuk, M. Mass spectrometry characterization of 3-OH butyrated β-cyclodextrin. Journal of Polymer Science Part A: Polymer Chemistry, 48, 5581-5592, 2010.

Peptu C., Balan-Porcarasu M., Siskova A., Skultety L., Mosnacek J. Cyclodextrins tethered with oligolactides-Green synthesis and structural assessment. Beilstein Journal of Organic Chemistry, 13, 779-792, 2017.

Peptu C., Danchenko M., Skultety L., Mosnacek J. Structural Architectural Features of Cyclodextrin Oligoesters Revealed by Fragmentation Mass Spectrometry Analysis. Molecules, 23, 2259, 2018.

Barner-Kowollik C., Gruendling T., Falkenhagen J., Weidner S. Mass spectrometry in polymer chemistry. John Wiley & Sons, Germany, 2012.

Montaudo G., Samperi F., Montaudo M.S. Characterization of synthetic polymers by MALDI-MS. Prog. Polym. Sci. 31, 277-357, 2006.

Dodero A., Schlatter G., Hebraud A., Vicini S., Castellano M. Polymer-free cyclodextrin and natural polymer-cyclodextrin electrospun nanofibers: A comprehensive review on current applications and future perspectives. Carbohydrate Polymers, 264, 118042, 2021.

Celebioglu A., Uyar T. Cyclodextrin nanofibers by electrospinning. Chemical Communications, 46, 6903-6905, 2010.

Rizzarelli P., Carroccio S. Modern mass spectrometry in the characterization and degradation of biodegradable polymers. Analytica Chimica Acta, 808, 18-43, 2014.

Jalabert M., Fraschini C., Prud'homme R.E. Synthesis and Characterization of Poly(L-Lactide)s and Poly(D-Lactide)s of Controlled Molecular Weight. Journal of Polymer Science Part A Polymer Chemistry, 45, 1944-1955, 2007.

Sosnowski S., Lewinski P. L-Lactide Polymerization Catalyzed by Tin(II) 2-Ethyl-Hexanoate. A Deeper Look at Chain Transfer Reactions. Polymer Chemistry, 6, 6292, 2015.

Topuz F., Kilic M.E., Durgun E., Szekely G. Fast-dissolving antibacterial nanofibers of cyclodextrin/antibiotic inclusion complexes for oral drug delivery. Journal of Colloid and Interface Science, 585, 184-194, 2021.